A multi-proxy record of MIS 11-12 deglaciation and glacial MIS 12 instability from the Sulmona Basin (central Italy)

Eleonora Regattieri[1,*], Biagio Giaccio[1], Paolo Galli[1,2], Sebastien Nomade[3], Edoardo Peronace[1], Paolo Messina[1], Andrea Sposato[1], Chiara Boschi[4], Maurizio Gemelli[5]

[1]Istituto di Geologia Ambientale e Geoingegneria, CNR, Via Salaria km 29.4, Monterotondo, Rome, Italy
[2]Dipartimento della Protezione Civile, Via Vitorchiano 4, 00189 Rome, Italy
[3]Laboratoire des Sciences du Climat et de l'Environnement, IPSL, laboratoire CEA/CNRS/UVSQ, Gif-Sur-Yvette, France
[4]Istituto di Geoscienze e Georisorse IGG-CNR, Via Moruzzi 1 Pisa, Italy
[5]Dipartimento di Scienze della Terra, University of PisaVia S. Maria 53 56126, Pisa Italy
*Corresponding author, eleonora.regattieri@igag.cnr.it

Abstract

A multi-proxy record (lithology, XRF, $CaCO_3$ content, $\delta^{18}O$ and $\delta^{13}C$) was acquired from a sediment core drilled in the intermountain Sulmona basin (central Italy). Tephrostratigraphic analyses of three volcanic ash layers ascribe the investigated succession to the MIS 12-MIS 11 period, spanning the interval ca. 500-410 ka. Litho-pedo facies assemblage indicates a predominant lacustrine deposition, interrupted by a minor sub-aerial and lake low stand episode. Variations in trace elements concentrations are related to changes in the clastic input to the lake. The oxygen isotopic composition of carbonate intervals is interpreted mainly as a proxy for the amount of precipitation in the high-altitude catchment of the karst recharge system. The record shows pronounced hydrological instability at orbital and millennial time-scales, which appears closely related to the Northern Hemisphere summer insolation pattern and replicates the North Atlantic and west Mediterranean Sea Surface Temperature (SST) fluctuations. The MIS 12 glacial inception is marked by an abrupt reduction of precipitation, lowering of the lake level and enhanced catchment erosion. A well-defined and isotopically prominent interstadial could be related to insolation maxima-precession minima at ca. 465 ka. This interstadial ends abruptly at ca. 457 ka and it is followed by a phase of strong short-

term instability. Drastic lake reduction and enhanced clastic flux characterized the MIS 12 glacial maximum. Lacustrine deposition starts again about 440 ka ago. The MIS 12-MIS 11 transition is characterized by a rapid increase in the precipitation, deepening of the lake level and reduction in the clastic input, interrupted by a short and abrupt return to drier conditions. Comparison with marine records from the Iberian margin and western Mediterranean suggests that major events of ice rafted debris deposition, related to southward migrations of the polar front, match the harshest periods in central Italy. This indicates strong teleconnections between Northern hemisphere ice sheet dynamics, North Atlantic oceanic conditions and Mediterranean continental hydrology.

Keywords: Stable isotope, lacustrine succession, MIS 12-11, tephrostratigraphy, Central Italy

1. Introduction

The marine isotope stage (MIS) 12-11 interval (460–380 ka, Railsback et al., 2015) encompasses the most extreme conditions of the last half million years of Earth's climate history, and occurred at a time when orbital configuration was similar to the most recent glacial-interglacial cycle (i.e., similar amount of solar radiation due to similar orbital eccentricity, Healey and Thunnell, 2004). In particularly, the glacial MIS 12 stands out as one of the most severe periods of the Late Quaternary, based on both marine (e.g., Shackleton, 1987; Raymo et al., 1990; Rohling et al., 1998; Poli et al., 2000; Bauch and Herlenkeuser, 2003; Toucanne et al., 2009; Billups et al., 2006; Lambert et al., 2012, Bard and Rickaby, 2009; Stein et al., 2009; Lang and Wolff, 2011; Girone et al., 2013; Naafs et al., 2013, 2014; Vásquez-Riveiros et al., 2013; Rohling et al., 2014) and continental archives (e.g. Tzedakis et al., 2003; Hughes et al., 2006, 2007, 2010; Russo-Ermolli et al., 2010), as well as in the Antarctica ice cores (Masson-Delmotte et al., 2010). Global ice volume was ~15% greater than during the last glacial maximum (LGM; ~30-20 ka), resulting in sea-levels about 140 m below present one (e.g. Shackleton, 1987; Rohling et al., 1998, 2014; Lisiecki and Raymo, 2005). On the contrary,

during the MIS 11, sea level is estimated to have been much higher than the current sea level. Even if sea level estimates are difficult to reconstruct, it has been suggested that during MIS 11 it may have reach 20 m above that of the present day (e.g. Hearty et al., 1999; Rohling et al., 2014), implying that ice caps were significantly smaller than during Holocene. Thus, glacial Termination V represents the highest-amplitude climatic shift since 600 ka (e.g. Howard, 1997; Healey and Thunnell, 2004). Paradoxically, this large glacial/interglacial change took place during a period when insolation changes were relatively small and precessional forcing was low (Imbrie and Imbrie, 1980; Raymo, 1997).

Evidence for millennial-scale instability during MIS 12 has been provided from both high latitude and sub-tropical North Atlantic marine records (e.g. Oppo et al., 1998; McManus et al., 1999; Poli et al., 2000; Chaisson et al., 2002; Haley and Thunnell, 2004; Billups et al., 2006, 2011; Stein et al., 2009; Voelker et al., 2010; Rodrigues et al., 2011; Vásquez-Riveiros et al., 2013; Naafs et al., 2013, 2014). The periodic occurrence of major ice-rafting events, analogous to the Heinrich Events during MIS 2 and MIS 3 (e.g. Hemming, 2004), is observed within MIS 12 in high latitude North Atlantic marine cores (e.g. Oppo et al., 1998; McManus et al., 1999; Hodell et al., 2008; Vásquez-Riveiros et al., 2013). Major ice-rafted debris (IRD) peaks were recognized also in the eastern and western mid-latitude North Atlantic (e.g. Stein et al., 2009; Voelker et al., 2010; Naafs et al., 2014) as far as south 34°N (Poli et al., 2000). This suggests that, because of the large ice-volume, the polar front would have migrated further south compared with the Last Glacial, directly influencing the mid-latitude North Atlantic (e.g. Poli et al., 2000; Billups et al., 2006; Naafs et al., 2014) and the Mediterranean sea hydrography (Girone et al., 2013), with an overall imprint on the global climate (Naafs et al., 2014). However, palaeoclimatic reconstructions for MIS 12 outside the North Atlantic region are scarce and mostly confined to the marine realm (e.g. Lourens et al., 2004, Bard and Rickaby, 2009; Maiorano et al., 2013; Girone et al., 2013), making it difficult to evaluate the extra-regional expressions of MIS 12 climate variability. In particular, only few studies document climatic changes

during this time interval in the Mediterranean region, especially from continental archives (e.g. Tzedakis et al., 2003, 2006; Hughes et al., 2006, 2007; Russo-Ermolli et al., 2009; Blain et al., 2012). Nevertheless, these data suggest that the MIS 12 maximum was particularly harsh in this region, with several small ice caps over the Balkans (Hughes et al., 2006) and major reductions in the arboreal vegetation of southern Europe (e.g. Tzedakis et al., 2003, 2006; Russo-Ermolli et al., 2009).

Many palaeoclimatic records in the Mediterranean have highlighted that changes in North Atlantic oceanic conditions were expressed in the region mainly as hydrological variations, with cold North Atlantic events and weakened Meridional Overturning Circulation (MOC) coinciding with drier conditions in the basin (e.g. Tzedakis et al., 2003; Drysdale et al., 2005, 2007, 2009; Regattieri et al., 2014a,b, 2015). This applies to both long-term glacial-interglacial changes and millennial-scale variability. Specifically, the sensitivity of the central Mediterranean hydrology to North Atlantic conditions is well documented for the Holocene (e.g. Zanchetta et al., 2007, 2014; Regattieri et al., 2014a), the Last Interglacial complex, i.e., the MIS 5 (e.g. Drysdale et al., 2005, 2007, 2009; Milner et al., 2012, 2013; Leng et al., 2013; Regattieri et al., 2014b, 2015) and the MIS 19 (Giaccio et al., 2015). However, the relationships between high-latitude climate and hydrological variability in the Mediterranean are still poorly known for the Lower-Middle Pleistocene (e.g. Tzedakis, 2003; Girone et al., 2013). With the aim to extend our knowledge on the North Atlantic-Mediterranean climatic teleconnections for the Middle Pleistocene period, we have assembled a multiproxy record ($\delta^{18}O$ and $\delta^{13}C$, $CaCO_3$ content and XRF data) of hydrological and environmental variability from a lacustrine sedimentary succession in the Sulmona basin (central Italy, Fig. 1), tephrochronologically constrained to the MIS 12-11 interval. The sequence has allowed us to reconstruct regional hydrological changes occurring at the orbital scale (i.e., glacial/interglacial transition), to investigate the occurrence of millennial-scale variability during MIS 12, and to explore teleconnections between Mediterranean hydrological variability and North Atlantic oceanic conditions during glacial inception, full glacial and deglaciation times.

2. Site description

2.1 Tectonic and stratigraphic setting

The Sulmona basin (Fig. 1) is a block-faulted intermontane depression formed during the Plio-Quaternary extensional tectonic phase (e.g. D'Agostino et al., 2001) and presently bounded by the active Mount Morrone, NW-SE-trending fault system (Gori et al., 2011; Galli et al., 2015) (Fig. 1). During the late Early-Upper Pleistocene, the basin was filled by a thick lacustrine-fluvial succession (e.g. Cavinato et al., 1994; Cavinato and Miccadei, 1995, 2000; Miccadei et al., 1998; Giaccio et al., 2012, 2013a). Lacustrine environment is documented until the Late Pleistocene (Giaccio et al., 2012, Regattieri et al., 2015), followed by alluvial-fan deposits of the Last Glacial (Gori et al., 2011) and minor Holocene colluvial and alluvial-fan episodes (Giaccio et al., 2012; Galli et al., 2015) (Fig. 1). The whole sedimentary infill of the Sulmona basin is very rich in tephra layers, which document the history of Italian explosive volcanoes and, through radiometric dating, allow a precise chronology of the successions to be established (e.g. Giaccio et al., 2012; 2013b, 2015; Sagnotti et al., 2014; Galli et al., 2015; Regattieri et al., 2015). Three main unconformity-bounded units compose the Sulmona Pleistocene succession, each chronologically constrained by magnetostratigraphy, tephrostratigraphy and an $^{40}Ar/^{39}Ar$ chronology to the intervals of ~814->530 ka (unit SUL6), ~530-<457 ka (unit SUL5), and ~110-14 ka (unit SUL4-3) (Giaccio et al., 2012, 2013a; 2013b; Sagnotti et al., 2014, Regattieri et al., 2015) (Fig. 1). The succession investigated in the present study belongs to unit SUL5, which was briefly described by Giaccio et al. (2009). For this present study, we investigated the ca. 12.5 m-thick interval of the SUL5 unit recovered in the upper part of a borehole (SC1, Giaccio et al., 2013a; Sagnotti et al., 2014) drilled throughout the SUL5 and SUL6 units. Unit SUL5 is characterized by the occurrence of several tephras (Fig. 1), such as: the Tufo di Bagni Albule (~527 ka), the Ash Fall-a (~517 ka) and the Pozzolane Rosse (~457 ka) marker layers from the Colli Albani caldera (Freda et al., 2011; Giaccio et al., 2013b) and the Fall A tephra (~500 ka) from the Sabatini volcanic

128 complex (Giaccio et al., 2014; Galli et al., 2015). The SUL5 unit is separated from the SUL6 unit by
129 an unconformity that, according to the local paleo-geomorphological setting, can be represented by
130 an erosional surface and/or a reddish-brownish paleosoil.

131 *2.2 Climatic and hydrological settings*

132 The Apennines represent a natural barrier in the central Mediterranean which traps eastward moving
133 moisture sourced from the Atlantic and the western Mediterranean. At present, about 60% of the
134 precipitation has a North Atlantic origin, especially during winter (e.g. Longinelli and Selmo, 2003)
135 and an inverse correlation is observed between rainfall amount and the North Atlantic Oscillation
136 (NAO) index (Lopez-Moreno et al., 2011). The site (Fig. 1) is influenced by the typical winter
137 Mediterranean storm-track trajectory (Lionello et al., 2006), with the most important centre of
138 cyclogenesis occurring in the Gulf of Genoa (Trigo et al., 2002). The basin topographic surface is
139 located between ca. 340 and 400 m a.s.l. The mean annual temperature is 13.7 °C, with an average
140 rainfall of ca. 870 mm (data from the Sulmona meteorological station). The amount-weighted mean
141 isotopic composition of the local precipitation can be assumed to be close to that measured at the
142 nearby (ca. 50 km) L'Aquila station (ca. 710 m a.s.l.), which is -7.13‰ (Longinelli and Selmo, 2003).
143 However, the main recharge for the Sulmona basin comes from a system of karst springs, which
144 dominate the hydrology of this sector of the Apennines (Barbieri et al., 2005; Desiderio et al., 2005a,
145 b) and likely represented the main source of recharge for the studied paleolake as well (Regattieri et
146 al., 2015; Giaccio et al., 2015). Recharge areas of these springs are located at higher altitudes (e.g.
147 mean altitude of recharge ca. 1200 and 1500 m asl, Barbieri et al., 2005; Desiderio et al., 2005a, b),
148 and therefore yield a $\delta^{18}O$ composition lower than local precipitation (e.g. Longinelli and Selmo,
149 2003). Due to orographic effects, precipitation reaches values of about 1200 mm at the summits areas
150 of the mountains feeding the basin. Longer rock-water interaction in the karst system leads to higher
151 concentrations of dissolved solids and high $\delta^{13}C$ of dissolved inorganic carbon (DIC) for the major

perennial springs compared to those draining more superficial sectors of the karst system (Falcone et al., 2008).

3. Methods

3.1 Sampling, sample preparation and $CaCO_3$ content

The present study focuses on the ca. 12.5 m-thick succession of core SC1, which was sampled at a resolution of ca. 10 cm between 0-7.7 m and of ca. 5 cm between 7.7-12.5 m. Samples were dried in an oven at 50 °C for 24 hours and carbonate content was obtained gasometrically on the bulk samples (i.e., not sieved). A subsample of the dried sample was gently disaggregated and sieved at 100 µm to separate biogenic remains (e.g. ostracods and shells) from the sediments. The fraction below 100 µm was powdered and homogenized for stable isotope and XRF analysis. The high $CaCO_3$ content throughout most of the studied interval suggests a total inorganic/total organic carbon ratio ≥0.3, a value which has been found to be a threshold for reliable measurements of the isotope composition of bulk carbonate samples (Oehlerich et al., 2013). Therefore, to reduce potential effects on isotopic measurement (Wierzbowski, 2007), no pre-treatment was performed before isotopic analyses. Samples corresponding to different stratigraphic facies were disaggregated with oxygen peroxide, then washed and sieved at 0.315 mm and investigated for paleontological content with a binocular microscope.

3.2 Stable isotope analysis

Stable isotope analyses were performed using a Gas Bench II (Thermo Scientific) coupled to a Delta XP IRMS (Finnigan) at the Institute of Geosciences and Earth Resources of the Italian National Research Council (IGG-CNR) of Pisa (Italy). Carbonate samples of ca. 0.15 mg of $CaCO_3$ were dissolved in H_3PO_4 (100%) for one hour at 70°C. All the results were reported to the relative VPDB international standard. Sample results were corrected using the international standard NBS-18 and a

176 set of three internal standards, previously calibrated using the international standards NBS-18 and
177 NBS-19. Analytical uncertainty for $\delta^{18}O$ and $\delta^{13}C$ were 0.17‰ and 0.15‰ respectively (2 σ).

178 *3.3 XRF analysis*

179 X-ray fluorescence spectrometry (XRF) analyses were performed at 20 cm resolution, using a NITON
180 XL3t GOLDD+ hand-held XRF unit (HHXRF) at the Earth Sciences Department of the University
181 of Pisa (Italy). During the analysis the instrument was set to'TestAllGeo' measurement modes, which
182 allowed the simultaneous detection of over eighteen elements heavier than Mg. The total counting
183 time for each sample was 142 seconds. The beam diameter was ~ 8 mm. Measured spectra were
184 converted to concentration using the Niton Data Transfer software. Performance of the NITON XL3t
185 is described in Gemelli et al., 2014.

186 *3.4 Tephrostratigraphic analyses*

187 Major-element composition was determined on micro-pumice fragments and/or glass shards from the
188 layers SUL 5a-9 and SUL 5b-1, which lay above the previously recognized Pozzolane Rosse tephra
189 (Fig. 2). Elemental analyses were carried out at the Institute of Environmental Geology and
190 Geoengineering of the Italian National Research Council (IGAG-CNR) (Rome, Italy) using a Cameca
191 SX50 electron microprobe analyzer equipped with a five-wavelength dispersive spectrometer.
192 Operating conditions and standards are provided in the Supporting information (Table S1).

193

194 **4. Results and interpretation**

195 *4.1 Tephrostratigraphy and chronological settings*

196 The investigated 12.5 m-thick interval in core SC1 contains three tephra layers (Fig. 2), including the
197 previously recognized Pozzolane Rosse marker tephra (9.20 m-depth in SC1 core, Fig. 2), dated by
198 the $^{40}Ar/^{39}Ar$ method at 457.4 ± 1.7 ka (2σ analytical uncertainty; Giaccio et al., 2013b, Table 1).
199 This interval occurs also in several outcropping sections surrounding the core SC1 site, where the

same tephrostratigraphic succession and lithostratigraphic features can be readily recognized. The uppermost tephra (SUL5a-9) occurs at 1.30 m of depth in SC1 core. SUL5a-9 is a 4 cm-thick layer mainly composed by transparent, glassy and highly vesicular micro-pumice with elongated bubbles associated with black, blocky glass shards and abundant K-feldspar and dark mica crystals. The glass shows a wide compositional range from high-K rhyolite (SiO_2 up to 71 wt%) to trachyte (SiO_2 59-61 wt%) (Fig. 3; full analytical data are provided in supplementary Table S1). In the Middle Pleistocene central Italy tephrostratigraphic record, high-K rhyolites are not common and represent peculiar characters of the earliest stage of the Vico volcano activity which has been dated between 419 and 403 ka (Period I of Perini et al., 2004). Specifically, layer SUL5a-9 can be correlated to the Vico α eruption (Cioni et al., 1987) which matches the Rio Ferriera Formation of Perini et al. (2004). This widespread tephra (Bigazzi et al., 1994; Marra et al., 2014) is dated at 419 ± 6 ka (2σ uncertainty) by Laurenzi and Villa (1987) and at 415 ± 6 ka (2σ uncertainty) by Marra et al. (2011). This last age was recalculated according to a different flux standard age to 419 ± 6 ka in Marra et al., (2014).

Tephra SUL5b-1 occurs at 5.15 m depth in SC1 core (Fig. 2, Table 1). It is up to 5 cm-thick, made of both whitish, moderately vesicular micropumice and grey purely vesicular microscoria associated with K-feldspar, clinopyroxene and dark-mica crystals. Glass from SUL5b-1, sampled in an outcropping section close to the SC1 drilling site, is trachytic in composition, with a relatively homogeneous content of SiO_2 (~62.5 wt%) and alkali sum (Na_2O+K_2O ~13-12 wt%). Although the Latium volcanoes, and especially the Sabatini and Vulsini complexes, could be considered the most probable sources for SUL5b-1 layer, due to their windward position with respect to the dominant stratospheric winds, and their relatively intense explosive activity in the time-span between c. 460 and 415 ka (e.g. Marra et al., 2014; Palladino et al., 2010), the relatively high content of Cl in glass from SUL5b-1(up to 0.4 wt%) is hardly compatible with these sources, that commonly are characterized by a very low Cl content (0.1 wt.%; e.g. Giaccio et al., 2014; Palladino et al., 2014). Relatively high content of chloride are instead rather common in glass from Campanian volcanoes.

In particular, even if not identical in the total alkali silica diagram, in terms of other major elements composition SUL5b-1 is similar to layer S2 from the Sessano basin (Fig. 3), Molise, southern Italy, dated by $^{40}Ar/^{39}Ar$ method at 437.9 ± 1.9 ka (2σ analytical uncertainty, Russo Ermolli et al., 2010, Table 1) and correlated to the Rio Rava eruption of the Roccamonfina caldera (Rouchon et al., 2008), which is located ca. 90 km southward from Sulmona basin. This tephra layer is rather widespread in southern Italy: it is thought to occur in several sedimentary sequences from southern Appennine intermontane depressions (e.g. Bojano, Mercure and Acerno basins; Aucelli et al., 2011; Giaccio et al., 2014, Petrosino et al., 2014; respectively).

These three tephras provide independent chronological control points and constrain the deposition of the investigated succession to between the glacial substages MIS12c, 12b and 12a, and the early MIS 11 substages 11e and 11d, following the recent nomenclature proposed by Railsback et al. (2015). For the tephrochronological purpose of the present study we adopt the age of 415 ± 6 ka for Vico α (Marra et al., 2011) because it was calculated using the same calibration used for the Pozzolane Rosse and S2-Rio Rava tephras (Table 1).

4.2 Lithology and $CaCO_3$ content

The general lithological and pedo-stratigraphic facies of the investigated interval of the SC1 core are shown in Fig. 2. From the base of the succession, at a depth of 12.40 m on the paleosol underlying SUL6 unit, up to a depth of 11.35 m, the sediments are composed by light brown, fine-grained massive calcareous marl (i.e., bio-mediated calcite, with $CaCO_3$ content between 80% and 20%, following the classification by Freytet and Verrecchia, 2002), with a $CaCO_3$ content between 70% and 80% (Fig. 2). From 11.35 m, the marls are darker and the $CaCO_3$ content decreases down to 20%. The paleontological association for this interval shows freshwater mollusks (e.g. *Bithinya tentaculata, Valvata cristata, Armiger crista*), rare ostracods and oogonia of *Chara spp*., indicating shallow lacustrine conditions. The interval between 11.05 m and 10.95 m depth is characterized by peat deposition and absence of $CaCO_3$ content, indicating shallowing of the lake level, with a brief

emergence of the core site, but with a persistently high water table. At 10.95 m green calcareous marl, with a $CaCO_3$ content of ca. 60-80 %, recurs. This interval contains the Pozzolane Rosse tephra (dated at 457 ± 2 ka, MIS 12b). At 7.65 m-depth, lacustrine deposition is abruptly interrupted by carbonate gravel with low content of silt matrix, followed by silty-sand deposits (at 7.45-6.45 m), likely related to sedimentary pulses from the alluvial fan systems originating from the high reliefs bounding the basin to the west (Fig. 1). Between 6.45 m and 5.20 m, rare mottles, root traces and millimetric carbonate concretions suggest a truncated soil profile with a Bk horizon (Retallack, 1990). Paleontological inspection reveals the presence of rare unidentified land snails shell fragments and some slug plates. The S2-Rio Rava tephra (438 ± 2 ka, MIS 12a) occurs at 5.15 m and marks the transition to another interval of lacustrine deposition, from 5.20 m to the top of the core (Fig. 2). It starts abruptly with an interval of calcareous grey-green marl, with the carbonate fraction progressively increasing towards the top and likely indicating a transition of the shore line at the core site and the progressive deepening of the lake. The paleontological association consists of abundant ostracods and freshwater mollusks, such as *Bithinya sp*. and *Pisidium sp*. From 3.15 m up to the core top, marls show a stable $CaCO_3$ content (between 70% and 90%) and faint laminations. The Vico α tephra (415 ± 6 ka, MIS 11c) occurs at 1.60 m.

In summary, it is possible to distinguish three main intervals within the core (Fig. 2):

i) Basal section [s-A], 12.40-7.70 m depth: Mostly composed by calcareous marl indicating persisting lacustrine deposition, interrupted by a lake level low-stand represented by the peat layer.

ii) Middle section s-B, 7.45- 5.20 m depth: Sediments of shoreline and alluvial-plain environments, indicating emergence of the core site due to a temporary restriction/disappearance of the lake.

iii) Uppermost section [s-C], 5.20-0.30 m depth: Mostly composed by carbonate marl, indicating lacustrine conditions and, possibly, progressive deepening of the lake.

SEM analyses show that the carbonate fraction of sections s-A and s-C is mainly composed by euhedral to sub-euhedral calcite crystals of ca. 10-15 μm, typical of authigenic deposition, i.e. carbonates precipitated directly from the lake water, mostly through biomediation influenced by physical conditions, such as hydrology and temperature (e.g. Kelts and Hu, 1978; Talbot, 1990; Kelts and Talbot, 1990; Leng and Marshall, 2004, Gierlowski-Kordesch, 2010).

4.3- The $\delta^{18}O$ records and its hydrological significance

For the Mediterranean region the final $\delta^{18}O$ of lake carbonates is thought to be determined by the isotopic composition of the local precipitation ($\delta^{18}O_p$) and by the residence time of water in the lake, which controls evaporation; temperature changes are thought to play only minor effects (e.g. Zanchetta et al., 1999; 2007b; 2012, Roberts et al., 2008; Leng et al., 2010, 2013). Indeed, following the classical Kim and O'Neil (1997) equation, the equilibrium isotope fractionation between carbonate and water has a gradient of ca -0.24‰/°C (between 10° and 40°C), which is mostly balanced by the gradient of +0.3‰/°C between mean annual $\delta^{18}O_p$ and temperature found by Bard et al. (2002) examining long-term rainfall data from the GNIP-IAEA stations of Genoa, Palermo and Pisa. Bard et al. (2002) also observed that the $\delta^{18}O_p$ in the central/western Mediterranean is negatively correlated with the amount of precipitation, with a slope of -2‰ per 100 mm/month. This so-called "amount effect" is considered to be the major driving factor for $\delta^{18}O$ of central Mediterranean lake carbonates (and speleothems), with lower $\delta^{18}O$ values associated with enhanced precipitation and higher values occurring during drier intervals (e.g. Bard et al., 2002; Drysdale et al., 2005, 2006, 2007, 2009; Roberts et al., 2008; Zanchetta et al., 2007a, 2007b, 2012, 2014; Leng et al., 2010, 2013; Regattieri et al., 2014, 2015). As discussed by Regattieri et al. (2015) and mentioned in section 2.1, most of the recharge for the Sulmona paleo-lake was related to a system of karst springs and it has been proposed that the $\delta^{18}O$ of lake waters was dominated under all conditions (i.e., both wetter and drier periods) by the isotopic composition of these spring waters, with the final $\delta^{18}O$ of lake carbonates reflecting mainly the $\delta^{18}O$ of precipitation in the high-altitude catchment areas (Regattieri

et al., 2015; Giaccio et al., 2015). This can be eventually modified by changes in the hydrological balance of the lake. However, according to the simple model proposed by Roberts et al. (2008), wetter periods lead to rapid replenishment of lake waters by recharge and shorter water residence times, thus reducing the effect of evaporation on the isotopic composition of the lake water. Instead, during drier phases and lower lake levels, residence time may be longer, producing higher lake-water isotopic values, thus acting in the same direction of the amount effect observed in rainfall.

Based on the above considerations, we therefore interpret the lacustrine $\delta^{18}O$ record from the MIS 12/MIS 11 section as principally driven by the amount of precipitation in the mountain areas feeding the Sulmona basin and, eventually, by changes in the lake hydrological budget, with lower values related to enhanced precipitation and higher values related to drier conditions. It may be argued that in some intervals $\delta^{18}O$ values of the bulk samples could be influenced by the detrital component, given the catchment is mostly composed of carbonate rocks. However, spot isotope analysis performed on gravels from the core and from nearby outcrops yield $\delta^{18}O$ values between -1.11 and +0.62 ‰ and $\delta^{13}C$ values between +1.50 ‰ and 2.50 ‰ (n=4), and can be readily discriminated from the authigenic carbonates (Fig. 4). This suggests that the observed variations throughout the record are not imputable to mixing between clastic and bio-mediated carbonate, thus supporting the notion that the authigenic calcite $\delta^{18}O$ signal dominates also where the clastic fraction is abundant.

The $\delta^{18}O$ record (Fig. 2) shows lower values between ca. -10.1 and -10.5 ‰, indicating wetter conditions, from the base of the sequence to 11.35 m. After the interruption of the $\delta^{18}O$ record, due to the occurrence of a peat layer, there is an abrupt increase of ca. 2.0 ‰ marking the onset of a drier period between 11.00 and 10.20 m. Then, precipitation seems to increase abruptly from depth 10.30 to 9.30 m, with $\delta^{18}O$ values returning to ca. -9 ‰. At 9.20 m there is another rapid jump to drier conditions ($\delta^{18}O$ values of ca. -7.0 ‰), followed by strong short-term variability on a trend of overall progressive climatic amelioration, reaching values of up to ca. -9.0 ‰ at 7.65 m. The presence of the Pozzolane Rosse tephra (ca. 457 ka) at 9.20 m suggests that this interval of pronounced hydrological instability corresponds to the MIS 12 glacial inception.

Between 7.65 m and 5.20 m (s-B, Fig. 2), the sedimentary facies suggests subaerial conditions, marked possibly by a short a depositional hiatus at the base (represented by the gravel layer). In this interval, bio-mediated precipitation is absent and most carbonate can be associated with pedogenesis. The $\delta^{18}O$ of these carbonates cannot be compared directly with lacustrine values (e.g. Cerling et al., 1984; Zanchetta et al., 2000; 2006) and thus for this interval we do not apply our interpretation to the $\delta^{18}O$ record. From 5.20 m to 3.55 m, the $\delta^{18}O$ values decreased rapidly from ca. -6.5‰ to ca. -10.0‰ (Fig. 2). This steep wetting trend is interrupted by an abrupt reversal to drier conditions centered at 4.10 m, preceded by a well-defined peak of lower values centered at 4.40 m. The presence of the S2-Rio Rava tephra (ca. 438 ka) at 5.15 m indicates that this prominent shift is consistent to the MIS 12/MIS 11 transition. The terminal portion of the record shows lighter and relatively invariant $\delta^{18}O$ values (average -9.5 ‰), with a slight trend toward increasing values from 1.90 m to the top of the sequence at 0.30 m (Fig. 2). The occurrence of Vico α tephra (1.30 m depth), dated at ca. 415 ka, allows us to tie this interval to the early part of the MIS 11 interglacial. Throughout the record several short-term events of reduced precipitation (Fig. 2) can be observed, especially during the first lacustrine phase (i.e., during the MIS 12 glacial), where they are marked by higher amplitude shifts.

4.4 The $\delta^{13}C$ record

In a lacustrine environment like Sulmona palaeolake, three predominant sources can affect the $\delta^{13}C$ of the total inorganic carbon (DIC), and consequently of the precipitating carbonates: (*i*) the isotope composition of the DIC of the inflowing waters; (*ii*) the rate of biological activity within the lake (i.e., photosynthesis and respiration); and (*iii*) the rate of recycling of organic matter within the lake and the CO_2 exchange between atmosphere and lake water (e.g. Hollander and Smith, 2001; Leng and Marshall, 2004; Zanchetta et al., 2012). The $\delta^{13}C$ of inflowing water comprises groundwater input and surface and sub-surface runoff. Today the larger karst springs in the area have high DIC $\delta^{13}C$ values (Falcone et al., 2008), which reflects predominantly CO_2 from the dissolution of the carbonate rocks in the catchment. Therefore, periods having high $\delta^{13}C$ values may indicate high karst spring

recharge and/or significant equilibration with atmospheric CO_2 (Leng and Marshall, 2004; Leng et al., 2010). On the contrary, CO_2 derived by decomposition of organic matter is significantly ^{13}C-depleted and large amount of soil CO_2 leached by waters (Deines, 1980) and/or mineralization of organic matter in the lake can yield lower DIC values. Soil CO_2 production is enhanced during warmer and wetter periods and reduced during intervals of climatic deterioration (e.g. Raich and Schlesinger, 1992), but changes in the lake level and/or trophic state can modify the rate between oxidation/burial of organic matter, affecting the final DIC isotopic budget of the lake (e.g. Zanchetta et al., 2007b). Combinations of these factors can have countering of reinforcing influences, so a simple interpretation in past environment is always not obvious.

In the interval from the base to ca. 7.70 m, $\delta^{13}C$ values are higher (from ca. -2.0 to ca 2.0 ‰) suggesting minor input from ^{13}C-depleted organic derived CO_2. From ca. 7.80 to 4.00 m the $\delta^{13}C$ record is characterised by progressively lower values (Fig. 2). Part of this interval corresponds to subaerial conditions, with the formation of pedogenic calcite, which is typically ^{13}C-depleted (Cerling and Quade, 1993; Zanchetta et al., 2000, 2006). When lake sedimentation recommences following subaerial exposure (s-B), the isotopic values are similar to that of the pedogenic carbonate, suggesting a large input from organic-derived CO_2, probably in a shallow lake with efficient recycling of organic matter (e.g. Zanchetta et al., 2012). The progressive increase of values associated with lower $\delta^{18}O$ from ca. 4.00 m to the top of the succession suggests the reactivation of karst spring with higher discharge at the beginning of MIS 11.

4.5- XRF

The concentration vs. depth profiles of the elements selected for the present study (Ti, K, Rb, Zr, Si, Sr, Ca) are shown in Fig. 2. In spite of the relatively low resolution of the XRF analyses (ca. 20 cm), the occurrence of the three tephra layers is clearly recognizable by increases of Ti, Rb, Zr, K and Si (Fig. 2). In the lacustrine sediments not containing tephra layers, Ti, K, Rb and Zr are usually indicative of minerogenic-clastic input to the lake and are thus considered as a reliable proxy for

aeolian (e.g. Yancheva et al. 2007; Voegel et al., 2010) or fluvial sedimentary input in the lacustrine systems (e.g. Minyuk et al. 2007; Voegel et al., 2010). The Sulmona catchment is mostly made of carbonate rocks (e.g. Cavinato and Miccadei, 2000) which contain only limited amount of these elements. Therefore the most likely sources are volcanoclastic deposits, which are abundant in the whole basin (e.g. Giaccio et al., 2009, 2012, 2013a), and/or exotic aeolian dust. Other elements could play multiple roles within the system depending on their individual chemistry and on variations in lake status. For example, Si is abundant in many alumino-silicate and volcanic minerals, but it is also associated with lake primary productivity, as it is a component of diatom frustules (e.g. Peinerud, 2000). Also, Sr can be associated with silicates, particularly plagioclase and feldspars, but it is related also to carbonate precipitation because it can substitute for Ca during $CaCO_3$ deposition.

As Ti content is mostly related to minerogenic input, the strength of its correlation to others elements results particularly useful for disentangling how they are associated with clastic transport into the lake (Fig. 5). All the considered elements except Ca and Sr are significantly positively correlated with Ti (Fig. 5), suggesting that their increase is closely related to this kind of transport. The highest positive correlations are observed between Ti and Zr ($R^2 = 0.86$; Fig. 5) and between Ti and Si ($R^2 = 0.72$; Fig. 5). Interestingly, Si shows a strongly negative correlation with Ca ($R^2 = 97$), suggesting that its primary source is volcanic, with a relatively low proportion of biogenic silica. Also, the positive correlations with Rb and K are significantly high ($R^2 = 0.68$ and 0.60, respectively; Fig. 5), which is expected because in volcanic mineral Rb covaries with K. The correlation between Ca and Ti on the other hand is strongly negative ($R^2 = 0.77$; Fig. 5), whereas Ca shows a very high positive correlation with $CaCO_3$ content ($R^2 = 0.97$, Fig. 5). Taken together, these two relationships indicate that the majority of Ca is related to carbonate minerals and that these minerals are not related to clastic input, supporting the notion that the carbonate fraction mostly derives from authigenic precipitation within the lake and thus yields a reliable $\delta^{18}O$ climate-driven signal. Sr correlates positively with both Ti ($R^2 = 0.41$; Fig. 5) and Ca ($R^2 = 0.45$, Fig. 5), indicating that its presence is related to both clastic input and to carbonate precipitation of dissolved Sr^{2+}.

Before discussing variations in the clastic input in our record and their potential relationship with climatic changes, we have to deal with dilution of the signal related to an increase in the amount of precipitating carbonates. Dilution in our record is indeed evident during phases of lacustrine deposition, where absolute abundances of all the investigated elements are lower compared to the phase of subaerial exposure (Fig. 2). Due to its abundance, conservative nature during transport and weathering and because it is not biologically important, Ti can be used to normalize the data of others elements (e.g. Kylander et al., 2011). Fig. 6 shows Zr/Ti and Rb/Ti ratios compared to the $\delta^{18}O$ depth-profile. Interestingly, the increases (decreases) in the clastic input in the lacustrine intervals (s-A and s-C) coincide with higher (lower) $\delta^{18}O$ values, i.e., to period of reduced/enhanced precipitation. Elemental ratios also increase during the phase of lowering of the lake level and subaerial exposure (Fig. 6). It has been shown that the Zr/Ti ratio can be used as a proxy for the intensity of wind and erosion in the lake catchment (e.g. Voegel et al., 2010; Kylander et al., 2011). The patterns of variability observed in our record are compatible with this interpretation, suggesting enhanced erosion and clastic transport during drier periods, likely related to reduction in vegetation cover and increasing wind intensity, although detailed analysis of the grain size would be required to further test this relationship. In this frame, it is interesting to note that for the Last Glacial, Giraudi et al. (2013) in discussing loess deposition over the Apennine, suggested long-distance transport. Our Zr/Ti ratio would suggest similar processes during MIS 12.

5. Discussion

5.1 Linking the Sulmona $\delta^{18}O$ record with North Atlantic climate variability

On orbital and millennial time scales, it has been proposed that changes in the precipitation amount, and thus in carbonate $\delta^{18}O$ composition, in the central and western Mediterranean are related to variations in the proportion of advected air masses from the Atlantic, which mostly depends on ocean SST variations (e.g. Drysdale et al., 2005, 2006, 2007, 2009; Zanchetta et al., 2007a, Regattieri et al.,

2014b, 2015). Under colder North Atlantic conditions, MOC weakened or stopped completely (e.g. Rasmussen et al., 1996; Curry and Oppo, 1997; Vidal et al., 1997) reducing evaporation and vapor transport to the western Mediterranean, leading to lower, ^{18}O-enriched, rainfall. Moreover, reduction of North Atlantic-sourced precipitation would lead to a higher proportion of vapor masses forming within the Mediterranean and having heavier $\delta^{18}O$ composition, due to reduced rainout fractionation and to evaporation from a more isotopically enriched water mass compared to the North Atlantic. This fact is noted in the studies of present day precipitation (Celle-Jeanton et al., 2001) and it is suggested to be important also on glacial/interglacial time scales (Marino et al., 2015). Conversely, strengthening of the MOC and warming of the North Atlantic cause greater evaporation and vapor transport to the western Mediterranean, thus increasing the total amount of precipitation and the proportion sourced from the North Atlantic- (i.e., more depleted), resulting in a lower $\delta^{18}O$ of rainfall. This is even more pronounced for the Apennines due to strong orographic effect (e.g. Drysdale et al., 2005). Particularly for the Sulmona carbonates, the independently-dated oxygen record from the early Last Glacial (115 to 90 ka, Regattieri et al., 2015) shows abrupt increases, indicative of reduced precipitation, during North Atlantic cold events C24 and C23 (e.g. McManus et al., 1994; Oppo et al., 2006). Further back in time, the Sulmona $\delta^{18}O$ time series of the MIS 19-20 interval (Giaccio et al., 2015) closely replicates the millennial-scale pattern of ice rafted debris (IRD) from North Atlantic site ODP-983 (Kleiven et al., 2011), as well as the major climatic shift occurring at the MIS 20/MIS 19 transition and matching the marine Termination IX (Giaccio et al., 2015). Therefore, we can confidently interpret the variability expressed by our MIS 12-MIS 11 $\delta^{18}O$ record as linked in the same way to North Atlantic conditions, with higher/lower $\delta^{18}O$ values related to colder/warmer North Atlantic, both on orbital and millennial time scales.

5.2 Orbital-scale variability

Unlike the $^{40}Ar/^{39}Ar$-based age models we developed for the MIS 5 and MIS 19-20 Sulmona records (Regattieri et al., 2015; Giaccio et al., 2015), a robust, independent chronology cannot be proposed

452 at this stage for the SUL5 unit. Although the three tephra layers dated at ca. 457 ka, 438 ka and 415
453 ka, provide strong and independent control points, the drastic changes in depositional environment,
454 i.e. from lacustrine to subaerial, and the occurrence of gravel layers - potentially associated to erosion
455 and/or a sedimentary hiatus (Fig. 2) - make hardly tenable any attempt to construct a reliable
456 continuous age model. Nevertheless, if we simply use these independently-dated control points to
457 link the Sulmona $\delta^{18}O$ depth series to the reference $\delta^{18}O$ global benthic stack (LR04, Lisieki and
458 Raymo, 2005, Fig. 7) and to the Northern Hemisphere summer insolation curve (Laskar et al., 2011;
459 Fig. 7), the general glacial-interglacial and orbital patterns appear well replicated in the Sulmona
460 hydrological record (Fig. 7). Even more interesting is the comparison with the Alkenone Sea Surface
461 Temperature (SST) record of core MD03-2699 from the western Iberian Margin (Fig. 7, Rodrigues
462 et al., 2011). Indeed the $\delta^{18}O$ record replicates quite well the general features of the temperature
463 record.
464 Previous works on the western Iberian margin have highlighted its importance for tracing North
465 Atlantic variability at orbital and millennial time-scales (e.g. Sanchez-Goni et al., 1999, 2008;
466 Shackleton et al., 2003, Voelker et al., 2010; Margari et al., 2010). During the MIS 12 glacial
467 inception, the abrupt decrease in SST, correlated to insolation minimum at ca. 474 ka, is expressed at
468 Sulmona as a period of reduced precipitation, marked by increasing $\delta^{18}O$ carbonate values and a
469 lowering of the lake level, as testified by peat deposition which itself represents the beginning, and
470 probably the most extreme portion, of this drier period. This interval is also marked by
471 contemporaneous increase of the clastic input (Fig. 6), likely indicating reduction in the vegetation
472 cover under colder and drier conditions.
473 The rapid increase of SST at ca. 470 ka appears to correlate in Sulmona with a period of enhanced
474 precipitation, marked by the return to lacustrine conditions, by the progressive deepening of the lake
475 level and by the drastic reduction of detrital input (Figs. 6 and 7). This condition ends at ca. 457 ka,
476 and it is near synchronous with the deposition of the Pozzolane Rosse tephra. It is worth noting that
477 this period appears more prominent in the hydrological record than in the temperature record, a feature

478 which was already observed in the Sulmona archive for the first interstadial of the early Last Glacial
479 (Regattieri et al., 2015). There, the pronounced hydrological signal was inferred to be in response to
480 prevailing winter precipitation (i.e., ^{18}O-depleted, Longinelli and Selmo, 2003). Enhanced seasonality
481 in the Mediterranean is thought to be related to teleconnections between the enhancement of the
482 boreal monsoon system during precession minima and consequently expansion of the mid-latitudes
483 high-pressure cells, responsible for summer aridity in the Mediterranean (e.g. Tzedakis et al., 2007;
484 Sanchez-Goni et al., 2008; Milner et al., 2012). Interestingly, also in the present record this prominent
485 peak could be correlated with precession minima at ca. 464 ka, suggesting that similar teleconnections
486 would have acted also for the MIS 12 glacial. The moderate SST decrease at ca. 454 ka corresponds
487 to another abrupt interval of climatic deterioration, followed by strong, short-term hydrological
488 variability in a general trend of increasing precipitation, which may correspond to the SST increase
489 starting around 450 ka (Fig. 7). Subaerial lithofacies of the section s-B indicate lowering of the lake
490 level, which can be related to pronounced decrease of regional precipitation consistent with the MIS
491 12 glacial maximum. Increase in the elemental ratios suggests also concomitant higher clastic input
492 that could be interpreted as reduction of the vegetation cover and/or enhanced wind activity.
493 Interestingly, a progressive increase of coarse-grained input through the MIS 13–12 interglacial–
494 glacial transition and during the MIS12 glacial maximum was reported for other intermontane
495 depressions located in the southern Apennines, such as the Mercure (Giaccio et al., 2014), the Sessano
496 (Russo-Ermolli et al., 2009), the Boiano (Amato et al., 2012) and the Acerno basins (Munno et al.,
497 2001; according to the revised chronology by Petrosino et al., 2014). Noteworthy is the correlation
498 between the Sulmona record and the sedimentary successions of these basins, which is underpinned
499 by the concomitant presence of the S2-Rio Rava tephra. Available low-resolution pollen data for the
500 Sessano and the Acerno basins also report a major reduction of the arboreal vegetation during the
501 MIS12 glacial, accompanied in the Sessano basin by a major desiccation phase (Russo-Ermolli et al.,
502 2009). This suggests that climatic changes during the glacial period should have had a regional
503 influence on sedimentary processes, corresponding to increase of the catchment erosion under colder

and drier conditions. It has been proposed that during the MIS 12 glacial maximum MOC stopped completely, due to large ice volume which suppressed deep water convection (e.g. Poli et al., 2000). The major phase of climate deterioration recorded by the Sulmona record suggests contemporaneous harsh conditions over the Apennines, strengthening the proposed link between AMOC conditions and Mediterranean hydrology.

The S2-Rio Rava tephra at ca. 438 ka marks the beginning of the subsequent reestablishment of the lacustrine environment (s-C). All the acquired proxies indicate a general trend toward climatic amelioration which can be related to the MIS 12/MIS 11 transition, i.e., the Termination V of the marine record. In Sulmona record, the deglaciation is characterized by a steep increase in the precipitation, responsible for rising of the lake level. Decreasing elemental ratios (Fig. 6) indicate that the clastic flux is limited by soil/vegetation development in the lake catchment. It is worth to recalling that similar $\delta^{18}O$ excursions in central Mediterranean continental carbonates records have been observed both during the MIS 6/MIS 5 transition (Drysdale et al., 2005, 2009; Regattieri et al., 2014b) and during the MIS 20/MIS 19 transition (Giaccio et al., 2015), the latter directly from the $\delta^{18}O$ of lake carbonates of the Sulmona basin. We would like to emphasize that the magnitude of the isotopic shift is similar for the three Apennine records (between 2.2 and 3.1 δ ‰). These shifts were previously interpreted as enhanced hydrological activity during deglaciation, related to North Atlantic warming *via* the amount effect. Strict similarities between MD03-2699 SST and SUL 5 $\delta^{18}O$ time series (Fig. 6) extend this interpretation to the MIS 12/MIS 11 transition. The final part of the record corresponds to the beginning of MIS 11 interglacial. High and stable oceanic SSTs are reflected in Sulmona record by high and steady precipitation, scarce clastic input and presumably high lake level. Enhanced carbonate precipitation, suggested by the highest $CaCO_3$ content, can be linked to increased lake productivity under favorable climatic conditions. Finally, high $\delta^{13}C$ values suggest high spring discharge, coherently with the proposed reconstruction. Interestingly, the climate-stratigraphical position of Vico α tephra in our record (i.e. within the interglacial) agrees well with the Paleo-Tiber

sedimentation reconstruction by Karner and Marra (2003), indeed in their sedimentary sequence this tephra marks the MIS11 high-stand.

5.3 Sub-orbital climate variability and integrated age-model for MIS 12-MIS 11 record

In addition to the orbital-related shifts in $\delta^{18}O$ values and of other proxy data discussed above (section 5.2), the record from the investigated interval of the SUL5 unit shows several short-term oscillations which potentially reflect sub-orbital (i.e., millennial) scale hydrological instability. Comparing the Sulmona $\delta^{18}O$ depth series with SST of core MD03-2699 (Rodrigues et al., 2012), it appears evident that the two records share similar pattern of variability also on shorter time-scale (Fig. 7). More specifically, the MIS 12 record from the Western Iberian Margin shows four pronounced cold events, related to reduced MOC, which lead the southward displacement of the Polar Front to the mid-latitudes of the North Atlantic. These events were associated to episodes of icebergs melting, with IRD deposition beyond the typical IRD belt (Rodrigues et al., 2012, Fig. 7).

Within the Mediterranean, these events were correlated with periods of reduced SST in the plankton-based records from Site ODP-975 (Balearic Sea, Girone et al., 2013, Fig.8) interpreted as resulting from polar water incursion into the Mediterranean via the Strait of Gibraltar during major phase of iceberg discharge (Girone et al., 2013, Fig. 8). These events can be tentatively correlated to intervals of increasing $\delta^{18}O$ values, indicating decreasing precipitation in the Sulmona basin and possibly enhanced lake evaporation. Quite straightforward is the identification of the first and last of these events, occurring at ca. 474 ka and 427 ka in the MD03-2699 time series, i.e., during the glacial inception and the deglaciation respectively. Similar IRD events during the early and late (i.e., deglacial) phase of major glaciations are a common feature of many North Atlantic records (e.g. McManus et al., 1999; Stein et al., 2009; Voelker et al., 2010; Naafs et al., 2013, 2014) and were related to critical thresholds in ice volume, which trigger major ice-sheet instability and iceberg surges (e.g. Tzedakis et al., 2012). In the multiproxy record of core U1313 from the central mid-latitude North Atlantic (Stein et al., 2009), the most prominent peaks in IRD are documented at the beginning

554 and at the end of the MIS 12, and are coeval to similar events recognized in the sub-polar record of
555 ODP-980 and M23414 (Oppo et al., 1998, McManus et al., 1999 and Vásquez-Riveiros et al., 2013
556 respectively). In U1313 they were interpreted as Heinrich-like events, i.e., with icebergs sourced from
557 the Hudson strait (Stein et al., 2009; Naafs et al., 2013), documenting episodes of enhanced iceberg
558 delivery into the central mid-latitude North Atlantic due to sudden instability of the Laurentide ice
559 sheet during a phase of major climate reorganization. These events appear to be expressed in our MIS
560 12 record, suggesting a high-level sensitivity of the isotope composition of the Sulmona lake
561 carbonates to hydrological changes linked to episodes of iceberg melting in response to large-scale
562 reorganization of surface circulation in the North Atlantic. These close relationship between North
563 Atlantic and Sulmona millennial-scale variability allows us to tune our depth-series to the temperature
564 record, and thus to fix, in addition to the tephras, further tie points useful for constructing a tentative
565 age model for the investigated interval of the SUL 5 unit.
566 To build our chronology, we thus integrated the three tephrochronologically-based independent
567 points with three additional tuning points from the SST record, visually chosen as the most similar
568 between the two curves (Fig. 7). We transfer their ages on the Sulmona $\delta^{18}O$ depth series and then
569 calculate two separate linear age models for the two lacustrine sub-units (s-A and s-C). The resulting
570 time series is show in Fig. 8. Bearing in mind the limitation of this approach, which provides just an
571 approximation, some general considerations can be drawn. First, the high-frequency variability
572 appears focused in the glacial portion of the record. The general trend of stable interglacial and
573 unstable glacial climate is a distinguish feature of most North Atlantic marine records for the MIS13-
574 MIS 11 period (e.g. McManus et al., 1999; Hodell et al., 2008; Stein et al., 2009; Rodrigues et al.,
575 2012), and the transition between the two modes in the marine records was suggested to occur when
576 the benthic $\delta^{18}O$, a proxy of the continental ice volume, exceeds the critical threshold of 4.15‰
577 (McManus et al., 1999). Interestingly, the interval of maximum instability in the Sulmona record
578 closely corresponds to the same time window (Fig. 8), suggesting a direct relationship between ice
579 sheet size and hydrological patterns in the Mediterranean. Another remarkable similarity could be

found between our record and the long pollen record from Tenaghi Philippon (Tzedakis et al., 2003, Fig. 8). The Tenaghi succession has an astronomically-calibrated timescale, based on the assumption that specific vegetation patterns are the results of distinctive orbital configurations (e.g. Magri and Tzedakis, 2000; Tzedakis et al., 2003). The chronology for the middle part of the SUL5 unit instead is primarily based on the independent tephra ages and only refined by tuning with sub-orbital events from the SST record of core MD03-2699 (Rodrigues et al., 2012), which is anchored to the marine LR04 chronology (Lisieki and Raymo, 2005). Therefore, the two age models are at least partially independent (although the LR04 chronology is, in turn, astronomically tuned). Orbital scale changes appear almost in phase in the two records, with increases/reductions of the arboreal vegetation at Tenaghi corresponding to increases/decreases of precipitation at Sulmona. Also, the amplitudes and frequencies of the millennial variability appear consistent, although large uncertainties and different resolutions prevent us for a comparison at this finer time-scale. Vegetation changes at Tenaghi are assessed to be related to northern summer insolation and to ice sheet size and configuration, through an ocean-atmospheric linkage which results in a spatial coherent pattern of climate variability between the high latitudes and the Mediterranean (e.g. Tzedakis et al., 2003). Taking into account that our age model is only partially dependent from orbital assumptions, the observed similarities between the Sulmona and Tenaghi records validates the correctness of our chronological approach and strengthen the notion of an *in-phase* Mediterranean response to hemispheric or global climatic variability, although with different amplitudes of the observed features (e.g. Tzedakis et al., 2003).

6. Concluding remarks

The multiproxy record ($\delta^{18}O$ and $\delta^{13}C$ from lacustrine carbonates, lithology and XRF) from the Sulmona basin, anchored to the period from ca. 500 to 410 ka by an age model primarily based on independent $^{40}Ar/^{39}Ar$ chronology, shows pronounced hydrological instability on both orbital and millennial time-scales. This variability strictly resembles coeval SST variations recorded in Western

Iberian margin and Mediterranean (Rodrigues et al., 2012). The isotope record shows an abrupt decrease in the precipitation from ca. 482 ka, corresponding to MIS 12 glacial inception. Lithological features and XRF data indicate a lowering of the lake level and enhanced catchment erosion, possibly due to a reduction in vegetation cover. This abrupt event can be related to significant climatic deterioration, expressed by North Atlantic SST decrease at 474 ka (Rodrigues et al., 2012) and by widespread IRD deposition described in the central and mid-latitudes North Atlantic (e.g. Rodrigues et al., 2012; Naafs et al., 2014), indicating southward migration of the polar front, disruption of MOC and reduced evaporation and advection from the ocean to the Mediterranean. The precession minimum at ca. 464 ka marks a well-defined and isotopically pronounced interstadial. The noticeable amplitude of this interstadial is not evident in the SST record and suggests higher seasonality of the precipitation modulated by enhancement of the boreal monsoon system, as previously suggested for the Sulmona isotope record of the Early Last Glacial (Regattieri et al., 2015). A phase of drastic lake level lowering and enhanced clastic flux occurs during the MIS 12 glacial maximum and could be related to suppressed MOC, due to maximum ice volume. The MIS 12/MIS 11 transition starts as early as 437 ka, and it is characterized by a rapid increase in the precipitation, rising lake level, reestablishment of authigenic calcareous sedimentation and drastic reduction in clastic input. This steep trend of climatic improvement is interrupted by an abrupt return to drier conditions around 427 ka, which corresponds to a sharp decrease in SST and to a major IRD event widespread recognized in the North Atlantic (e.g. Vásquez-Riveiros et al., 2013). This event is followed by full interglacial conditions of MIS 11, which, in contrast with the abrupt and marked oscillations observed during the MIS 12 glacial, is characterized by a substantial stability.

The strict similarity between the Sulmona record and SST variations from the Iberian margin and in the Mediterranean (Fig. 8) during the investigated period provide evidences for strong teleconnections between central Mediterranean hydrology and North Atlantic conditions. Recently, it has been proposed that the hydrological significance of $\delta^{18}O$ of Mediterranean continental carbonates can be offset by effect of changes in the isotopic composition of the sea source (Rohling et al., 2015; Marino

et al., 2015). However, the major shifts in $\delta^{18}O$ values observed in the Sulmona record are stratigraphically and temporally strictly related to chemical and lithological variations, which are unambiguously related to hydrological changes. As corollary, the $\delta^{18}O$ variability must be considered as mainly related to the climatic change, thus strengthening its relevance as a powerful proxy for reconstructing the hydrological variability in the Mediterranean basin.

Acknowledgements

The authors would thanks G. Zanchetta for thorough discussion and support in the paleontological analysis and R.N. Drysdale for comments on early version of the manuscript. F. Bimbi is also thanked for laboratory help.

References

Amato V. Aucelli P. C., Russo Ermolli E., Rosskopf C. M., Cesarano M., Pappone G. 2012. Quaternary morpho-evolution, tectonic and environmental changes in the Boiano intermontane basin (central-southern Italy). Rendiconti Online Società Geologica Italiana 21, 1225-1227.

Aucelli P. Amato V., Baranello S., Cesarano M. 2011. Nuovi dati sull'evoluzione pleistocenica dei bacini intramontani di Boiano e di Sessano (Molise, Italia meridionale) di Boiano e di Sessano (Molise, Italia meridionale).

Barbieri M., Boschetti T., Petitta M., Tallini M. 2005. Stable isotope (^{2}H, ^{18}O and $^{87}Sr/^{86}Sr$) and hydrochemistry monitoring for ground water hydrodinamics analyses in a karst aquifer (Gran Sasso, Central Italy). Applied Geochemistry 20, 2063-2081.

Bard E., Delaygue G., Rostek F., Antonioli F., Silenzi S., Schrag D. 2002. Hydrological conditions in the western Mediterranean basin during the deposition of Sapropel 6 (ca. 175 kyr). Earth Planetary Sciences Letters 202, 481-494.

654 Bard E., Rickaby R. E. 2009. Migration of the subtropical front as a modulator of glacial climate.
655 Nature 460, 380-383.

656 Bauch H.A., Erlenkeuser H. 2003. Interpreting glacial–interglacial changes in ice volume and climate
657 from sub artic deep water foraminiferal $\delta^{18}O$. In: Droxler A.W., Poore R.Z., Burckle L.H. (Eds.),
658 Earth's Climate and Orbital Eccentricity. American Geophysical Union,Washington DC, USA, 87–
659 102.

660 Bigazzi G., Bonadonna F.P., Cioni R., Leone G., Sbrana A., Zanchetta G. 1994. Nuovi dati
661 geochimici, petrografici e geocronologici su alcune cineriti plio-pleistoceniche del Lazio e della
662 Toscana. Memorie descrittive della carta geologica d'Italia Vol. XLIX, 135-150.

663 Billups K., Lindley C., Fisler J., Martin P. 2006. Mid Pleistocene climate instability in the subtropical
664 northwestern Atlantic. Global and Planetary Change 54, 251-262.

665 Blain H. A., Cuenca-Bescós G., Lozano-Fernández I., López-García J. M., Ollé A., Rosell J.,
666 Rodríguez J. 2012. Investigating the Mid-Brunhes Event in the Spanish terrestrial sequence. Geology
667 40, 1051-1054.

668 Cavinato G.P., Cosentino D., De Rita D., Funiciello R., Parotto M. 1994. Tectonicsedimentary
669 evolution of intrapenninic basins and correlation with the volcano-tectonic activity in central Italy.
670 Memorie Descrittive della Carta Geologica d'Italia 49, 63–76.

671 Cavinato G.P., Miccadei E. 1995. Sintesi preliminare delle caratteristiche tettoniche e sedimentarie
672 dei depositi quaternari della conca di Sulmona (L'Aquila). Journal of Quaternary Science 8 129–140.

673 Cavinato G.P, Miccadei E. 2000. Pleistocene carbonate lacustrine deposits: Sulmona basin (central
674 Apennines, Italy). In Lake Basins Through Space and Time.

675 Celle-Jeanton H., Travi Y., Blavoux B. 2001. Isotopic typology of the precipitation in the Western
676 Mediterranean region at three different time scales. Geophysical Research Letters 28, 1215-1218.

677 Cerling T. E. 1984. The stable isotopic composition of modern soil carbonate and its relationship to
678 climate. Earth and Planetary Science Letters, 71(2), 229-240.

679 Cerling T. E., Quade, J. 1993. Stable carbon and oxygen isotopes in soil carbonates. Climate change
680 in continental isotopic records, 217-231.

681 Chaisson W.P., Poli M.S., Thunell, R.C. 2002. Gulf stream and western boundary undercurrent
682 variations during MIS 10–12 at site 1056, Blake-Bahama Outer Ridge. Marine geology 189(1), 79-
683 105.

684 Cioni R., Sbrana A., Bertagnini A., Buonasorte G., Landi P., Rossi U., Salvati L. 1987.
685 Tephrostratigraphic correlations in the Vulsini, Vico and Sabatini volcanic successions. Periodico di
686 Mineralogia 56(2-3), 137-155.

687 Curry W.B., Oppo, D.W. 1997. Synchronous, high-frequency oscillations in tropical sea surface
688 temperatures and North Atlantic Deep Water production during the last glacial cycle.
689 Paleoceanography 12(1), 1-14.

690 D'Agostino N., Jackson J.A., Dramis F., Funiciello R. 2001. Interactions between mantle upwelling,
691 drainage evolution and active normal faulting: an example from the central Apennines (Italy).
692 Geophysical Journal International 147, 475-497

693 Deines P. 1980. The isotopic composition of reduced organic carbon. Handbook of environmental
694 isotope geochemistry, 329-406.

695 Desiderio G., Rusi S., Tatangelo F. 2005a: Utilizzo di tecniche isotopiche (^{18}O e ^{2}H) nello studio delle
696 acque sotterranee in aree protette dell'Appennino Abruzzese. Rivista italiana di Agrometeorologia
697 9/1, 90-91.

698 Desiderio G., Ferracuti L., Rusi S., Tatangelo F. 2005b. Il contributo degli isotopi naturali ^{18}O e ^{2}H
699 nello studio dell idrostrutture carbonatiche abruzzesi e delle acque mineralizzate nell'area abruzzese
700 e molisana. Giornale di Geologia Applicata 2, 453-458.

701 Drysdale R.N., Zanchetta G., Hellstrom J.C., Fallick A.E., Zhao J.X. 2005. Stalagmite evidence for
702 the onset of the Last Interglacial in southern Europe at 129+/−1 ka. Geophysical Research Letters 32,
703 1-4.

704 Drysdale R.N., Zanchetta G., Hellstrom J.C., Fallick A.E., McDonald J., Cartwright I. 2007.
705 Stalagmite evidence for the precise timing of North Atlantic cold events during the Early Last Glacial,
706 Geology 35, 77-80.

707 Drysdale R.N., Zanchetta G., Hellstrom J.C., Fallick A.E., Sanchez Goni M.F., Couchoud I.,
708 McDonald J., Maas R., Lohmann G., Isola I. 2009. Evidence for obliquity forcing of glacial
709 termination II. Science 325, 1527-1531.

710 Falcone R.A., Falgiani A., Parisse B., Petitta M., Spizzico M., Tallini M. 2008. Chemical and isotopic
711 ($\delta^{18}O‰$, $\delta^{2}H‰$, $\delta^{13}C‰$, ^{222}Rn) multi-tracing for groundwater conceptual model of carbonate aquifer
712 (Gran Sasso INFN underground laboratory-central Italy). Journal of Hydrology 357, 368-388.

713 Freda C., Gaeta M., Giaccio B., Marra F., Palladino D.M., Scarlato P., Sottili G. 2011. CO_2-driven
714 large mafic explosive eruptions: the Pozzolane Rosse case study from the Colli Albani volcanic
715 district (Italy). Bulletin of Volcanology 73, 241–256.

716 Freytet P., Verrecchia E. P. 2002. Lacustrine and palustrine carbonate petrography: an overview.
717 Journal of Paleolimnology 27(2), 221-237.

718 Galli P., Giaccio B., Peronace E., Messina P. 2015. Holocene Paleoearthquakes and Early–Late
719 Pleistocene Slip Rate on the Sulmona Fault (Central Apeninnes, Italy). Bulletin of the Seismological
720 Society of America. 10.1785/0120140029

721 Gemelli M., D'Orazio M., Folco L. 2015. Chemical Analysis of Iron Meteorites Using a Hand-Held
722 X-Ray Fluorescence Spectrometer. Geostandards and Geoanalytical Research 39(1), 55-69.

723 Giaccio B., Messina P., Sposato A., Voltaggio M., Zanchetta G., Galadini F., Gori S., Santacroce R.
724 2009. Tephra layers from Holocene lake sediments of the Sulmona Basin, central Italy: implications
725 for volcanic activity in Peninsular Italy and tephrostratigraphy in the central Mediterranean area.
726 Quaternary Science Reviews 28(25), 2710-2733.

727 Giaccio B., Nomade N., Wulf S., Isaia R., Sottili G., Cavuoto G., Galli P., Messina P., Sposato A.,
728 Sulpizio R., Zanchetta G. 2012. The late MIS 5 Mediterranean tephra markers: a reappraisal from
729 peninsular Italy terrestrial records. Quaternary Science Reviews 56, 31-45.

730 Giaccio B., Castorina F., Nomade S., Scardia G., Voltaggio M., Sagnotti L., 2013a. Revised
731 chronology of the Sulmona lacustrine succession, central Italy. Journal of Quaternary Science 28,
732 545-551.

733 Giaccio B., Arienzo I., Sottili G., Castorina F., Gaeta M., Nomade S., Galli P., Messina P. 2013b.
734 Isotopic (Sr-Nd) and major element fingerprinting of distal tephras: an application to the Middle-Late
735 Pleistocene markers from the Colli Albani volcano, central Italy. Quaternary Science Reviews 67,
736 190-206.

737 Giaccio B., Galli P., Peronace E., Arienzo I., Nomade S., Cavinato G.P., Mancini M., Messina P.,
738 Sottili G. 2014. A 560–440 ka tephra record from the Mercure Basin, southern Italy: volcanological
739 and tephrostratigraphic implications. Journal of Quaternary Science, 29(3), 232-248.

740 Giaccio B., Regattieri E., Zanchetta G., Nomade S., Renne P.R., Sprain C.J., Drysdale R.N., Tzedakis
741 P.C., Messina P., Scardia G., Sposato A., Bassinot F. 2015. Duration and dynamics of the best orbital
742 analogue to the present interglacial. Geology. In press, doi: 10.1130/G36677.1 |

743 Gierlowsky-Kordesch E.H. 2010. Lacustrine carbonates. in Developments in Sedimentology 61, 2-
744 50.

745 Giraudi C., Zanchetta G., Sulpizio R. 2013. A Late-Pleistocene phase of Saharian dust deposition in
746 the high Apennine mountains (Italy). Alpine Mediterranean Quaternary 26, 110-122.

747 Girone A., Maiorano P., Marino M., Kucera M. 2013. Calcareous plankton response to orbital and
748 millennial-scale climate changes across the Middle Pleistocene in the western Mediterranean.
749 Palaeogeography, Palaeoclimatology, Palaeoecology 392, 105-116.

750 Gori S., Giaccio B., Galadini F., Falcucci E., Messina P., Sposato A., Dramis F. 2011. Active normal
751 faulting along the Mt. Morrone south-western slopes (central Apennines, Italy). International Journal
752 of Earth Sciences 100, 157-171.

753 Healey S., Thunell R. 2004. Millennial-scale variability in western subtropical North Atlantic surface
754 and deep water circulation during marine isotope stages 11 and 12. Paleoceanography, 19(1).

755 Hearty P.J., Kindler P., Cheng H., Edwards R.L. 1999. A+ 20 m middle Pleistocene sea-level
756 highstand (Bermuda and the Bahamas) due to partial collapse of Antarctic ice. Geology 27(4), 375-
757 378.

758 Hemming S.R. 2004. Heinrich events: Massive late Pleistocene detritus layers of the North Atlantic
759 and their global climate imprint. Reviews of Geophysics 42(1).

760 Hodell D.A., Channell J.E., Curtis J.H., Romero O.E., Röhl U. 2008. Onset of "Hudson Strait"
761 Heinrich events in the eastern North Atlantic at the end of the middle Pleistocene transition (~ 640
762 ka)?. Paleoceanography, 23(4).

763 Hollander D.J., Smith M.A. 2001. Microbially mediated carbon cycling as a control on the $\delta^{13}C$ of
764 sedimentary carbon in eutrophic Lake Mendota (USA): new models for interpreting isotopic
765 excursions in the sedimentary record. Geochimica et Cosmochimica Acta 65, 4321–4337.

766 Howard W.R. 1997. Palaeoclimatology: A warm future in the past. Nature 388(6641), 418-419.

767 Hughes P.D., Gibbard P.L., Woodward J.C. 2006. Middle Pleistocene glacier behaviour in the
768 Mediterranean: sedimentological evidence from the Pindus Mountains, Greece. Journal of the
769 Geological Society 163(5), 857-867.

770 Hughes P.D., Woodward J.C., Gibbard, P.L. 2007. Middle Pleistocene cold stage climates in the
771 Mediterranean: new evidence from the glacial record. Earth and Planetary Science Letters 253(1),
772 50-56.

773 Hughes P.D., Woodward J.C., Van Calsteren P.C., Thomas L.E., Adamson K.R. 2010. Pleistocene
774 ice caps on the coastal mountains of the Adriatic Sea. Quaternary Science Reviews 29(27), 3690-
775 3708.

776 Imbrie J., Imbrie J.Z. 1980. Modeling the climatic response to orbital variations. Science 207(4434),
777 943-953.

778 Karner D.B., Marra F. 2003. $^{40}Ar/^{39}Ar$ dating of glacial Termination V and the duration of marine
779 isotopic stage 11. Earth's Climate and Orbital Eccentricity: The Marine Isotope Stage 11 Question,
780 61-66.

781 Kelts K., Hsü K.J. 1978. Freshwater carbonate sedimentation. In Lakes, Chemistry, Geology, Physics,
782 (ed.). Lerman A Springer-Verlag: Berlin, 295–323.

783 Kelts K., Talbot M. 1990. Lacustrine carbonates as geochemical archives of environmental change
784 and biotic/abiotic interactions. In Large Lakes (pp. 288-315). Springer Berlin Heidelberg.

785 Kim S.T., O'Neil J.R. 1997. Equilibrium and nonequilibrium oxygen isotope effects in synthetic
786 carbonates. Geochimica et Cosmochimica Acta 61(16), 3461-3475.

787 Kleiven H.F., Hall I.R., McCave I.N., Knorr G., and Jansen E., 2011. Coupled deep-water flow and
788 climate variability in the middle Pleistocene North Atlantic. Geology 39, 343–346.

789 Kylander M. E., Ampel L., Wohlfarth B., Veres D. 2011. High-resolution X-ray fluorescence core
790 scanning analysis of Les Echets (France) sedimentary sequence: new insights from chemical proxies.
791 Journal of Quaternary Science 26(1), 109-117.

792 Lambert F., Bigler M., Steffensen J.P., Hutterli M., Fischer H. 2012. Centennial mineral dust
793 variability in high-resolution ice core data from Dome C, Antarctica. Climate of the Past 8 (2), 609-
794 623.

795 Lang N., Wolff E.W., 2011. Interglacial and glacial variability from the last 800 ka in marine, ice and
796 terrestrial archives. Climate of the Past 7 361-380

797 Laskar J., Fienga A., Gastineau M., Manche, H. 2011. La2010: a new orbital solution for the long-
798 term motion of the Earth. Astronomy & Astrophysics, 532, A89.

799 Laurenzi M.A., Villa I.M., 1987. $^{40}Ar/^{39}Ar$ chronostratigraphy of Vico ignimbrites.Period. Mineral.
800 56, 285-293.

801 Leng M., Marshall J.D. 2004. Palaeoclimate interpretation of stable isotope data from lake sediment
802 archives. Quaternary Science Reviews 23, 811–831.

803 Leng M.J., Baneschi I., Zanchetta G., Jex C., Wagner H., Vogel H. 2010. Late Quaternary
804 palaeoenvironmental reconstruction from Lakes Ohrid and Prespa (Macedonia/Albania border) using
805 stable isotopes. Biogeosciences 7, 1347-1359.

806 Leng M.J., Wagner B., Boehm A., Panagiotopoulos K., Vane C.H., Snelling A., Haidon C., Woodley
807 E., Voegel H., Zanchetta G., Baneschi, I. 2013. Understanding past climatic and hydrological
808 variability in the Mediterranean from Lake Prespa sediment isotope and geochemical record over the
809 Last Glacial cycle. Quaternary Science Reviews 66, 123-136.

810 Lionello P., Bhend J., Buzzi A., Della-Marta P.M., Krichak S., Jansà A., Maheras P., Sanna A., Trigo
811 I.F., Trigo R. 2006. Cyclones in the Mediterranean region: climatology and effects on the
812 environment. In P. Lionello, P. Malanotte-Rizzoli, R. Boscolo (eds) Mediterranean Climate
813 Variability. Amsterdam: Elsevier (NETHERLANDS), 324-272.

814 Lisiecki L.E., Raymo M.E. 2005. A Pliocene-Pleistocene stack of 57 globally distributed benthic $\delta^{18}O$
815 records. Paleoceanography 20 PA1003.

816 Longinelli A., Selmo E., 2003. Isotopic composition of precipitation in Italy: a first overall map.
817 Journal of Hydrology 270, 75-88.

818 López-Moreno J.I., Vicente-Serrano S.M., Morán-Tejeda E., Lorenzo-Lacruz J., Kenawy A.,
819 Beniston M. 2011. Effects of the North Atlantic Oscillation (NAO) on combined temperature and
820 precipitation winter modes in the Mediterranean mountains: Observed relationships and projections
821 for the 21st century. Global and Planetary Change 77, 62–76.

822 Lourens L.J. 2004. Revised tuning of Ocean Drilling Program Site 964 and KC01B (Mediterranean)
823 and implications for the δ18O, tephra, calcareous nannofossil, and geomagnetic reversal chronologies
824 of the past 1.1 Myr. Paleoceanography, 19(3).

825 Magri D., Tzedakis P.C. 2000. Orbital signatures and long-term vegetation patterns in the
826 Mediterranean. Quaternary International 73/74, 69–78.

827 Maiorano P., Tarantino F., Marino M., De Lange G.J. 2013. Paleoenvironmental conditions at Core
828 KC01B (Ionian Sea) through MIS 13–9: evidence from calcareous nannofossil assemblages.
829 Quaternary International 288, 97-111.

830 Marino G., Rohling E.J., Rodríguez-Sanz L., Grant K.M., Heslop D., Roberts A.P., Stanford J.D.,
831 Yu, J. (2015). Bipolar seesaw control on last interglacial sea level. Nature 522(7555), 197-201.

832 Marra F., Deocampo D., Jasckson M.D., Ventura G., 2011. The Alban Hills and Monti Sabatini
833 volcanic products used in ancient Roman masonry (Italy): an integrated stratigraphic, archaeological,
834 environmental and geochemical approach. Earth Science Reviews 108, 115e136

835 Marra F., Sottili G., Gaeta M., Giaccio B., Jicha B., Masotta M., Palladino D.M., Deocampo D.M.
836 2014. Major explosive activity in the Monti Sabatini Volcanic District (central Italy) over the 800–
837 390 ka interval: Geochronological–geochemical overview and tephrostratigraphic implications.
838 Quaternary Science Reviews 94, 74-101.

839 Margari V., Skinner L.C., Tzedakis P.C., Ganopolski A., Vautravers M., Shackleton N.J. 2010. The
840 nature of millennial-scale climate variability during the past two glacial periods. Nature Geoscience
841 3(2), 127-131.

842 Masson-Delmotte V., Stenni B., Pol K., Braconnot P., Cattani O., Falourd S., Jouzel J., Landais A,
843 Minster B., Barnola J.M., Chappellaz J., Krinner G., Johnsen S., Röthlisberger R., Hansen J.,
844 Mikolajewicz, U., Otto-Bliesner, B. 2010. EPICA Dome C record of glacial and interglacial
845 intensities. Quaternary Science Reviews 29(1), 113-128.

846 McManus J. F., Oppo D.W., Cullen J. L. 1999. A 0.5-million-year record of millennial-scale climate
847 variability in the North Atlantic. Science 283(5404), 971-975.

Miccadei E., Barberi R., Cavinato G.P. 1998. La geologia quaternaria della conca di Sulmona (Abruzzo, Italia centrale). Geologica Romana 34, 59–86.

Milner A.M., Collier R.E., Roucoux K.H., Müller U.C., Pross J., Kalaitzidis S., Tzedakis P.C. 2012. Enhanced seasonality of precipitation in the Mediterranean during the early part of the Last Interglacial. Geology 40, 919-922.

Milner A.M., Müller U.C., Roucoux K.H., Collier R.E., Pross J., Kalaitzidis S., Christianis K., Tzedakis P.C. 2013. Environmental variability during the Last Interglacial: a new high-resolution pollen record from Tenaghi Philippon, Greece. Journal of Quaternary Science 28, 113-117.

Minyuk P.S., Brigham-Grette J., Melles M., Borkhodoev V.Y, Glushkova O.Y. 2007. Inorganic geochemistry of El0gygytgyn Lake sediments (northeastern Russia) as an indicator of paleoclimatic change for the last 250 kyr. Journal of Paleolimnology 37, 123–133

Munno R., Petrosino P., Romano P., Russo Ermolli E., Juvigné É. 2001. A late Middle Pleistocene climatic cycle in southern Italy inferred from pollen analysis and tephrostratigraphy of the Acerno lacustrine succession. Géographie physique et Quaternaire 55(1), 87-99.

Naafs B.D.A., Hefter J., Stein R. 2013. Millennial-scale ice rafting events and Hudson Strait Heinrich(-like) Events during the late Pliocene and Pleistocene: a review. Quaternary Science Reviews 80, 1-28.

Naafs B.D.A., Hefter J., Stein R. (2014). Dansgaard-Oeschger forcing of sea surface temperature variability in the midlatitude North Atlantic between 500 and 400 ka (MIS 12). Paleoceanography 29(11), 1024-1030.

Oehlerich M., Baumer M., Lücke A., Mayr C. 2013. Effects of organic matter on carbonate stable isotope ratios (δ13C, δ18O values)–implications for analyses of bulk sediments. Rapid Communications in Mass Spectrometry 27, 707-712.

871 Oppo D.W., McManus J.F., Cullen J.L. 1998. Abrupt climate events 500,000 to 340,000 years ago:
872 Evidence from subpolar North Atlantic sediments. Science 279(5355), 1335-1338.

873 Palladino D.M., Simei S., Sottili G., Trigila R. 2010. Integrated approach for the reconstruction of
874 stratigraphy and geology of Quaternary volcanic terrains: an application to the Vulsini Volcanoes
875 (central Italy). Geological Society of America Special Papers 464, 63-84.

876 Palladino D.M., Gaeta M., Giaccio B., Sottili, G. 2014. On the anatomy of magma chamber and
877 caldera collapse: the example of trachy-phonolitic explosive eruptions of the Roman Province (central
878 Italy). Journal of Volcanology and Geothermal Research 281, 12-26.

879 Peinerud E.K. 2000. Interpretation of Si concentrations in lake sediments: three case studies.
880 Environmental Geology 40, 64–72.

881 Perini G., Francalanci L., Davidson J.P., Conticelli S. 2004. Evolution and genesis of magmas from
882 Vico Volcano, Central Italy: multiple differentiation pathways and variable parental magmas. Journal
883 of Petrology 45(1), 139-182.

884 Petrosino P., Jicha B.R., Mazzeo F.C. Russo-Ermolli E. 2014. A high resolution tephrochronological
885 record of MIS 14–12 in the Southern Apennines (Acerno Basin, Italy). Journal of Volcanology and
886 Geothermal Research 274, 34-50.

887 Poli M.S., Thunell R.C., Rio D., 2000. Millennial-scale changes in North Atlantic Deep Water
888 circulation during marine isotope stages 11 and 12: Linkage to Antarctic climate. Geology 28 (9) 807-
889 810.

890 Raich J.W., Schlesinger, W.H. 1992. The global carbon dioxide flux in soil respiration and its
891 relationship to vegetation and climate. Tellus 44(2), 81-99.

892 Railsback R.B., Gibbard P.L., Head, M.J., Voarintsoa N.R.G., Toucanne S. 2015 An optimized
893 scheme of lettered marine isotope substages for the last 1.0 million years, and the climatostratigraphic
894 nature of isotope stages and substages Quaternary Science Reviews 111, 94-106.

895 Rasmussen T.L., Thomsen E., Labeyrie L., van Weering T.C. 1996. Circulation changes in the
896 Faeroe-Shetland Channel correlating with cold events during the last glacial period (58–10 ka).
897 Geology 24(10), 937-940.

898 Raymo M. E. 1997. The timing of major climate terminations. Paleoceanography 12(4), 577-585.

899 Regattieri E., Zanchetta G., Drysdale R., Isola I., Hellstrom J., Dallai, L. 2014a. Lateglacial to
900 Holocene trace element record (Ba, Mg, Sr) from Corchia Cave (Apuan Alps, central Italy):
901 paleoenvironmental implications. Journal of Quaternary Science 29(4), 381-392.

902 Regattieri E., Zanchetta G., Drysdale R.N., Isola I., Hellstrom J.C., Roncioni A. 2014b. A continuous
903 stable isotope record from the penultimate glacial maximum to the Last Interglacial (159–121ka)
904 from Tana Che Urla Cave (Apuan Alps, central Italy). Quaternary Research 82, 450–461.

905 Regattieri E., Giaccio B., Zanchetta G., Drysdale R.N., Galli P., Nomade S., Peronace E., Wulf S.
906 2015. Hydrological variability over the Apennines during the Early Last Glacial precession minimum,
907 as revealed by a stable isotope record from Sulmona basin, Central Italy. Journal of Quaternary
908 Science 30(1), 19-31.

909 Retallack G.J., Dugas D.P., Bestland E.A. 1990. Fossil soils and grasses of a Middle Miocene East
910 African grassland. Science 247(4948), 1325.

911 Roberts N., Jones M.D., Benkaddur A., Eastwood W.J., Filippi M.L., Frogley M.R., Lamb H.F.,
912 Leng M.J., Reed J.M., Stein M., Stevens L., Valero-Garcès B., Zanchetta G. 2008. Stable isotope
913 records of Late Quaternary climate and hydrology from Mediterranean lakes: the ISOMED
914 synthesis. Quaternary Science Review 27, 2426-2441.

915 Rodrigues T., Voelker A.H.L., Grimalt J.O., Abrantes F. Naughton F. 2011. Iberian Margin sea
916 surface temperature during MIS 15 to 9 (580–300 ka): glacial suborbital variability versus interglacial
917 stability. Paleoceanography 26(1).

918 Rohling E.J., Fenton M., Jorissen F.J., Bertrand P., Ganssen G., Caulet J.P. 1998. Magnitudes of sea-
919 level lowstands of the past 500,000 years. Nature 394 (6689), 162-165.

920 Rohling E.J., Foster G.L., Grant K.M., Marino G., Roberts A.P., Tamisiea M.E., Williams F. 2014.
921 Sea-level and deep-sea-temperature variability over the past 5.3 million years. Nature 508 (7497),
922 477-482.

923 Rohling E.J., Marino G., Grant K.M. 2015. Mediterranean climate and oceanography, and the
924 periodic development of anoxic events (sapropels). Earth Science Reviews 143, 62-97.

925 Rouchon V., Gillot P.Y., Quidelleur X., Chiesa S., Floris B. 2008. Temporal evolution of the
926 Roccamonfina volcanic complex (Pleistocene), central Italy. Journal of Volcanology and Geothermal
927 Research 177, 500–514.

928 Russo-Ermolli E., Aucelli P.P., Di Rollo A., Mattei M., Petrosino P., Porreca M., Rosskopf C.M.
929 2010. An integrated stratigraphical approach to the Middle Pleistocene succession of the Sessano
930 basin (Molise, Italy). Quaternary International 225(1), 114-127.

931 Sagnotti L., Scardia G., Giaccio B., Liddicoat J.C., Nomade S., Renne P.R., Sprain C.J. 2014.
932 Extremely rapid directional change during Matuyama-Brunhes geomagnetic polarity reversal.
933 Geophysical Journal International 199, 1110-1124.

934 Sanchez-Goñi M.F., Eynaud E., Turon J.L., Shackleton N.J. 1999. High resolution palynological
935 record off the Iberian margin: direct land-sea correlation for the Last Interglacial complex. Earth and
936 Planetary Science Letters 171, 123-137.

937 Sánchez Goñi M.F., Landais A., Fletcher W.J., Naughton F., Desprat S., Duprat J. 2008. Contrasting
938 impacts of Dansgaard–Oeschger events over a western European latitudinal transect modulated by
939 orbital parameters. Quaternary Science Reviews 27, 1136-1151.

940 Shackleton N.J. 1987. Oxygen isotopes, ice volume and sea level. Quaternary Science Reviews 6 (3-
941 4), 183-190.

942 Shackleton N.J., Sanchez-Goñi M.F., Pailler D., Lancelot Y. 2003. Marine Isotope Substage 5e and
943 the Eemian Interglacial. Global and Planetary Change 36, 151–155.

944 Stein R., Hefter J., Grützner J., Voelker A., Naafs, B.D.A. 2009. Variability of surface water
945 characteristics and Heinrich-like events in the Pleistocene midlatitude North Atlantic Ocean:
946 Biomarker and XRD records from IODP Site U1313 (MIS 16–9). Paleoceanography, 24(2).

947 Talbot M.R. 1990. A review of the palaeohydrological interpretation of carbon and oxygen isotopic
948 ratios in primary lacustrine carbonates. Chemical Geology: Isotope Geoscience Section 80(4), 261-
949 279.

950 Toucanne S., Zaragosi S., Bourillet J.F., Gibbard P.L., Eynaud F., Giraudeau J., Turon J.-L., Cremer
951 M., Cortijo E., Martinez P., Rossignol L. 2009. A 1.2 Ma record of glaciation and fluvial discharge
952 from the West European Atlantic margin. Quaternary Science Reviews 28, 2974-2981.

953 Trigo I.F., Bigg G.R., Davies T.D. 2002. Climatology of cyclogenesis mechanisms in the
954 Mediterranean. American Metereological Society 130, 549-569.

955 Tzedakis P.C., McManus J.F., Hooghiemstra H., Oppo D.W., Wijmstra T.A. 2003. Comparison of
956 changes in vegetation in northeast Greece with records of climate variability on orbital and suborbital
957 frequencies over the last 450 000 years. Earth and Planetary Science Letters 212(1), 197-212.

958 Tzedakis P.C., Hooghiemstra H., Pälike H. 2006. The last 1.35 million years at Tenaghi Philippon:
959 revised chronostratigraphy and long-term vegetation trends. Quaternary Science Reviews 25(23),
960 3416-3430.

961 Tzedakis P.C. 2007. Seven ambiguities in the Mediterranean palaeoenvironmental narrative."
962 Quaternary Science Reviews 26, 2042-2066.

963 Tzedakis P.C., Wolff E.W., Skinner L.C., Brovkin,V., Hodell D.A., McManus, J.F., Raynaud D.
964 2012. Can we predict the duration of an interglacial?. Climate of the Past 8(5), 1473-1485.

965 Vásquez-Riveiros N., Waelbroeck C., Skinner L., Duplessy J.C., McManus J.F., Kandiano E.S.,
966 Bauch H. A. 2013. The "MIS 11 paradox" and ocean circulation: Role of millennial scale events.
967 Earth and Planetary Science Letters 371, 258-268.

968 Vidal L., Labeyrie L., Cortijo E., Arnold M., Duplessy J.C., Michel E., Van Weering T.C.E. 1997.
969 Evidence for changes in the North Atlantic Deep Water linked to meltwater surges during the
970 Heinrich events. Earth and Planetary Science Letters 146(1), 13-27.

971 Voelker A.H., Rodrigues T., Billups K., Oppo D., McManus J., Stein R., Hefter J., Grimalt J.O. 2010.
972 Variations in mid-latitude North Atlantic surface water properties during the mid-Brunhes (MIS 9–
973 14) and their implications for the thermohaline circulation. Climate of the Past 6, 531-552.

974 Vogel H., Wagner B., Zanchetta G., Sulpizio R., Rosén P. 2010. A paleoclimate record with
975 tephrochronological age control for the last glacial-interglacial cycle from Lake Ohrid, Albania and
976 Macedonia. Journal of Paleolimnology 44(1), 295-310.

977 Wierzbowski H. 2007. Effects of pre-treatments and organic matter on oxygen and carbon isotope
978 analyses of skeletal and inorganic calcium carbonate. International Journal of Mass Spectrometry
979 268, 16–29.

980 Yancheva G., Nowaczyk N.R., Mingram J., Dulski P., Schettler G., Negendank J.F.W., Liu J., Sigman
981 D.M., Peterson L.C., Haug G.H. 2007. Influence of the intertropical convergence zone on the East
982 Asian monsoon. Nature 445 74–77.

983 Zanchetta G., Bonadonna F.P., Leone G. 1999. Stable isotope data on continental molluscs from Valle
984 di Castiglione, near Rome, Italy. 37 m record of paleoclimatological events. Quaternary Research 52,
985 293-299.

986 Zanchetta G., Vito M.D., Fallick A.E., Sulpizio R. 2000. Stable isotopes of pedogenic carbonates
987 from the Somma-Vesuvius area, southern Italy, over the past 18 kyr: palaeoclimatic implications.
988 Journal of Quaternary Science 15(8), 813-824.

989 Zanchetta G., Becattini R., Bonadonna F.P., Bossio A., Ciampalini A., Colonese A. Michelucci, L.
990 2006. Late middle Pleistocene cool non-marine mollusc and small mammal faunas from Livorno
991 (Italy). Rivista Italiana di Paleontologia e Stratigrafia 112, 135-155.

992 Zanchetta G., Drysdale R.N., Hellstrom J.C., Fallick A.E., Isola I., Gagan M., Pareschi M.T. 2007a.
993 Enhanced rainfall in the western Mediterranean during deposition of sapropel S1: stalagmite evidence
994 from Corchia Cave (Central Italy). Quaternary Science Reviews 26, 279-286.

995 Zanchetta G., Borghini A, Fallick AE, Bonadonna FP, Leone G. 2007b Late Quaternary
996 palaeohydrology of Lake Pergusa (Sicily, southern Italy) as inferred by stable isotopes of lacustrine
997 carbonates. Journal of Paleolimnology 38, 227-239.

998 Zanchetta G., van Welden A., Baneschi I., Drysdale R.N., Sadori L., Roberts N., Giardini M., Beck
999 C., Pascucci V., Sulpizio R. 2012. Multiproxy record for the last 4500 years from Lake Shkodra
1000 (Albania/Montenegro). Journal of Quaternary Science 27, 780-789.

1001 Zanchetta G., Bar-Matthews M., Drysdale R.N., Lionello P., Ayalon A., Hellstrom J.C., Isola I.,
1002 Regattieri E. 2014. Coeval dry events in the central and eastern Mediterranean basin at 5.2 and 5.6 ka

recorded in Corchia (Italy) and Soreq caves (Israel) speleothems. Global and Planetary Change 122, 130–139.

Name	Depth (m)	Correlated tephra	Source	Age (ka)	Uncertainty (ka) 2σ analytical.	Standard used and age
Pozzolane Rosse	9.20		Colli Albani	457.4*	1.7	ACs at 1.194 Ma equivalent to FCs at 28.02 Ma
Sul5b-1	5.15	Rio Rava/S2	Roccamonfina	437.9**	1.9	FCs at 28.02 Ma
Sul5a-9	1.30	Vico α	Vico	414.8***	6	FCs at 28.02 Ma

Table 1

Tables and Figures

Name	Depth (m)	Correlated tephra	Source	Age (ka)	Uncertainty (ka) 2σ analytical.	Standard used and age
Pozzolane Rosse	9.20		Colli Albani	457.4*	1.7	ACs at 1.194 Ma equivalent to FCs at 28.02 Ma
Sul5b-1	5.15	Rio Rava/S2	Roccamonfina	437.9**	1.9	FCs at 28.02 Ma
Sul5a-9	1.30	Vico α	Vico	414.8***	6	FCs at 28.02 Ma

1029 Table 1- Names, depths, correlated tephras, source areas and ages of tephra layers in the investigated
1030 succession. ACs (Alder Creek sanidine) $^{40}Ar/^{39}Ar$ standard with age of 1.194 Ma is equivalent to FCs
1031 (Fisher Canyon sanidine) at 28.02 Ma.

1032

1033

1034

1035

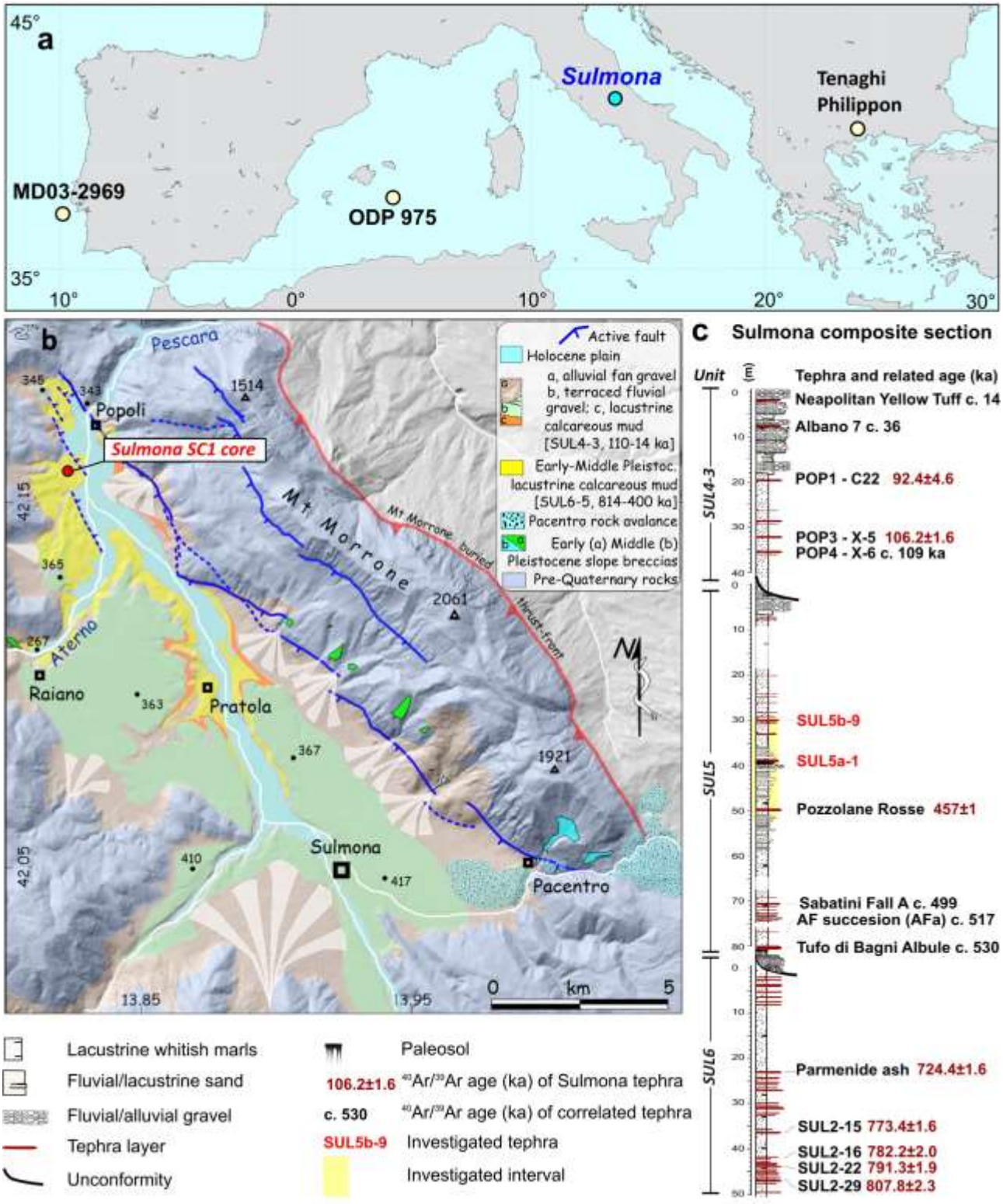

Figure 1- Reference map and geological and stratigraphic framework of the Sulmona basin. a) Location of the investigated Sulmona 5 (SUL5) unit investigated in this study, and of other palaeoclimatic records mentioned in the text. b) Simplified geological map of the Sulmona basin (from Galli et al., 2015); c) composite stratigraphic section of the three main unconformity bounded

1041 fluvio-lacustrine units, with the position of $^{40}Ar/^{39}Ar$ and tephrostratigraphic chronological
1042 constraints shown (from Giaccio et al., 2012; Giaccio et al., 2013a; 2013b; Sagnotti et al., 2014; Galli
1043 et al., 2015; Regattieri et al., 2015; Giaccio et al., 2015).

1044

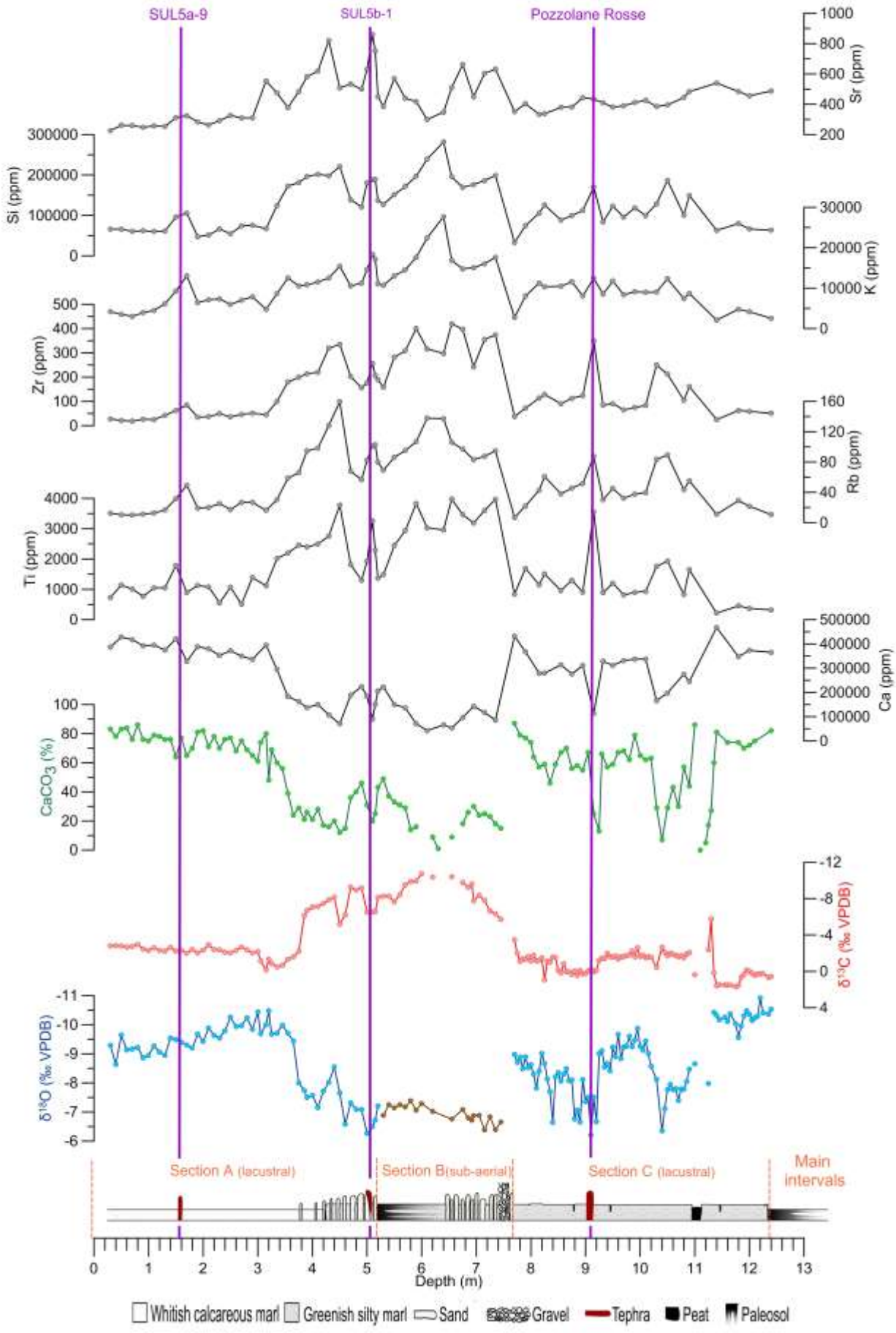
SUL5a-9
SUL5b-1
Pozzolane Rosse
Si (ppm)
Sr (ppm)
K (ppm)
Zr (ppm)
Rb (ppm)
Ti (ppm)
Ca (ppm)
CaCO3 (%)
δ13C (‰ VPDB)
δ18O (‰ VPDB)
Section A (lacustral)
Section B(sub-aerial)
Section C (lacustral)
Main intervals
Depth (m)
Whitish calcareous marl
Greenish silty marl
Sand
Gravel
Tephra
Peat
Paleosol

Figure 2- Stratigraphy and proxies depth series for the investigated portion of SC1 core. Purple lines indicate tephra layers. PR: Pozzolane Rosse tephra dated to 457.4 ± 1.7 ka (Giaccio et al., 2013b)

Figure 3- Total alkali vs silica and representative Harker diagrams (EMPA composition) for glass of the Sulmona tephra SUL5a-9 (column a) and SUL5b-1 (column b) and for their correlative tephra. Vico α EMPA glass composition of pumices from distal Vico α unit (Marra et al., 2014); Vico I Period: XRF composition of pumices from the basal pyroclastic units of Vico volcano (Perini et al., 2004); Tephra Vico: EDS glass composition from distal tephra (Valdarno, Tuscany) correlated to the basal units of Vico volcano (Bigazzi et al., 1994); Sessano-S2: EDS composition of glass from the layer S2 of the Sessano basin (Molise) correlated to the Rio Rava eruption of the Roccamonfina volcano (Russo-Ermolli et al., 2010).

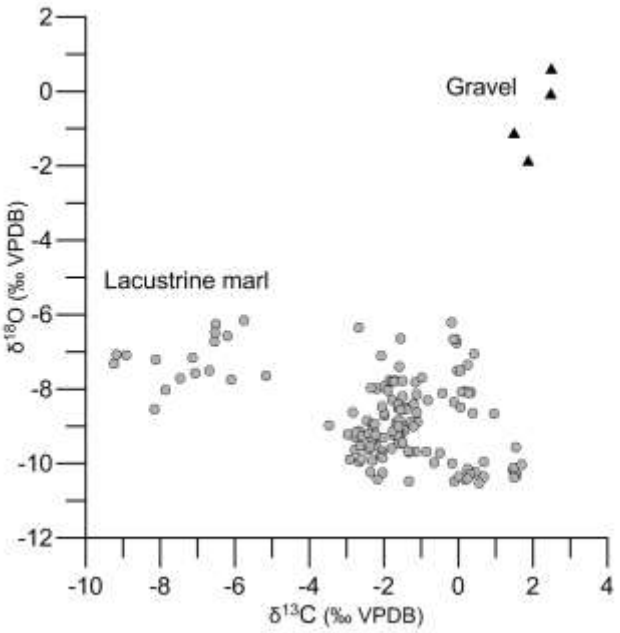

1065

1066 Figure 4- Plot of $\delta^{13}C$ vs $\delta^{18}O$ values of lacustrine carbonates and gravel from SC1 core and from

1067 nearby outcrops.

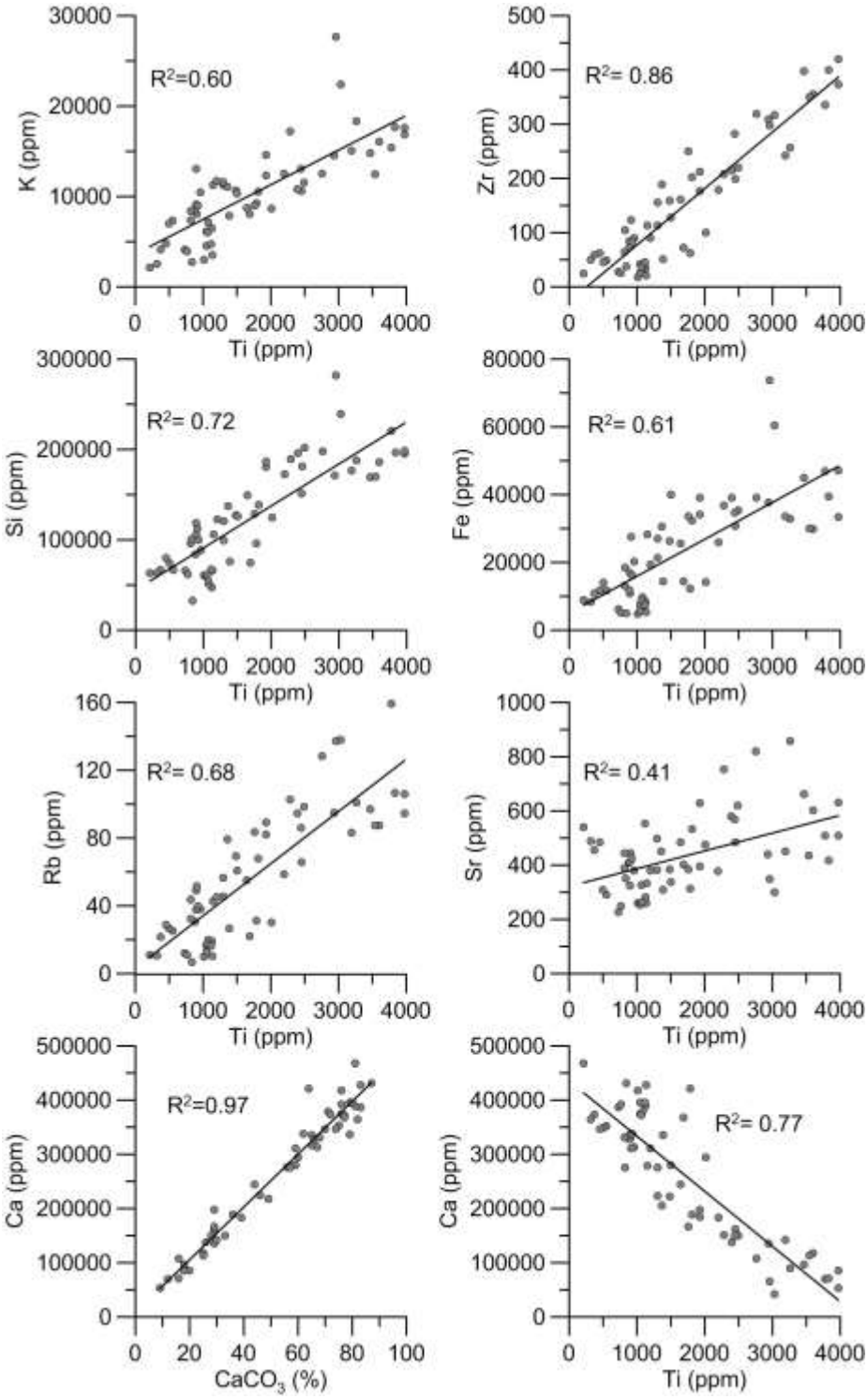

1068

1069 Figure 5- Correlation plots of Ti vs other elements and of Ca vs $CaCO_3$ content.

1070

1071

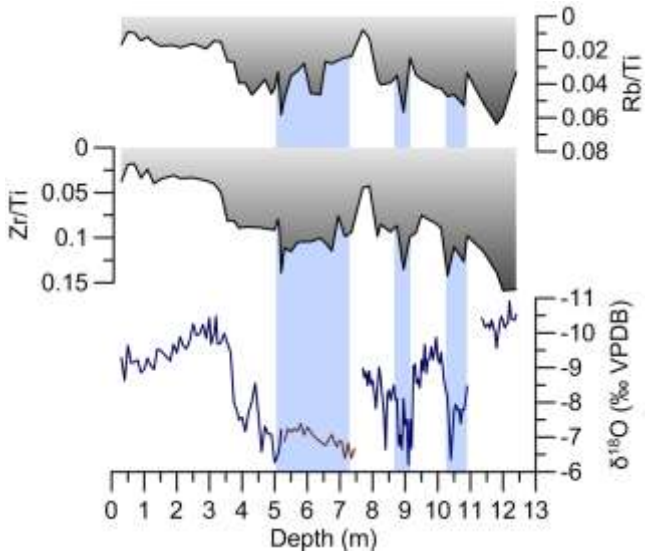

1072

1073 Figure 6- Depth series of Zr/Ti and Rb/Ti compared to $\delta^{18}O$ depth series (blue: lacustrine; brown:
1074 sub-aerial). Blue shading indicates periods of concomitant increase in clastic input and $\delta^{18}O$
1075 composition, see text for details.

1076

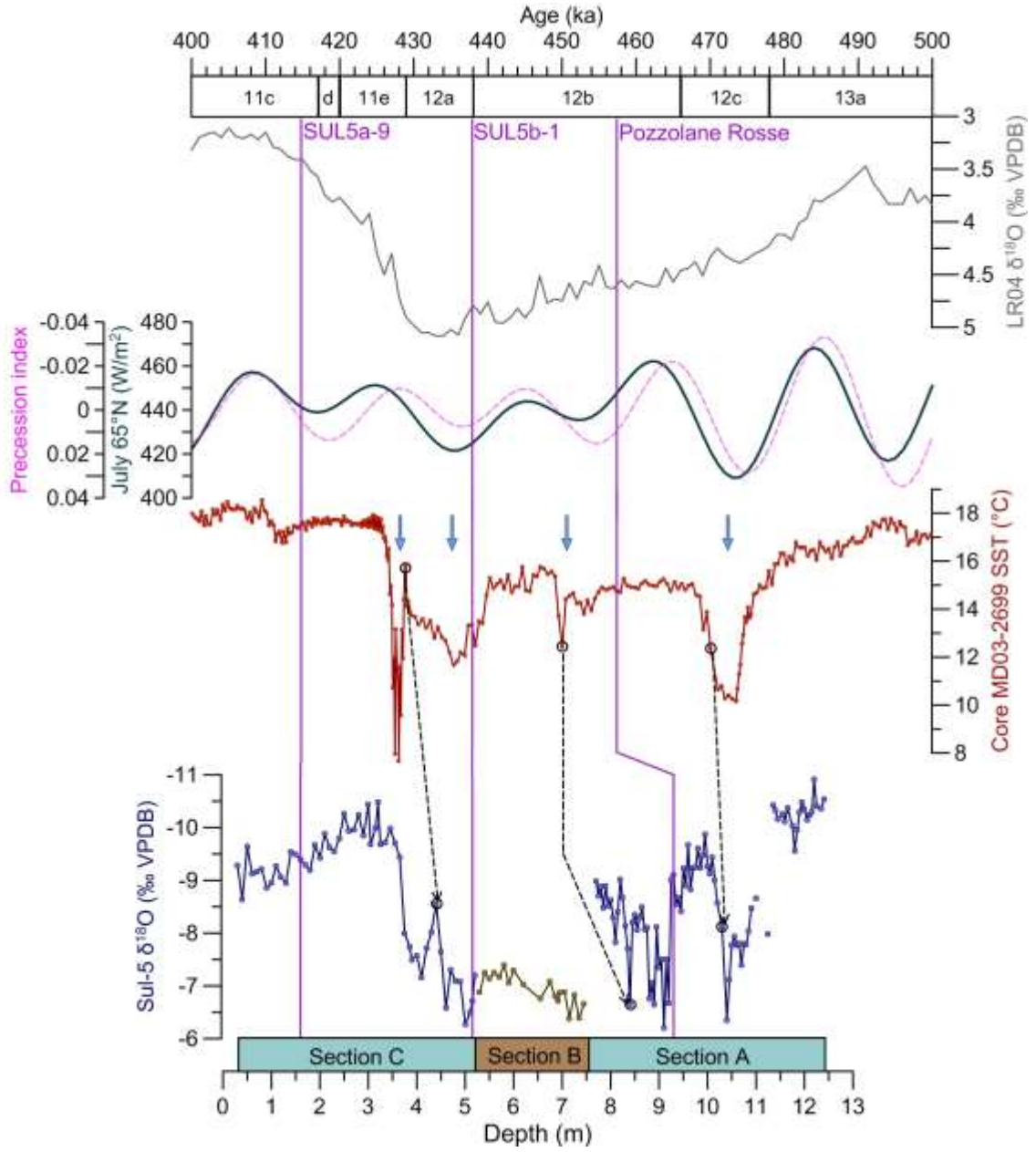

Figure 7- Bottom: stratigraphic sub-units, $\delta^{18}O$ (blue: lacustrine, brown: sub-aerial) and tephra layers (purple lines) of the investigated portion of core SC1 plotted vs depth. Ages of the tephra is used to anchor the depth series to the chronologybased on the recent nomenclature of stages and sub-stages (A, Railsback et al., 2015), to the LR04 benthic stack reference curve (B, Lisiecki and Raymo, 2005), to orbital parameters (C, precession index and July insolation at 65°N, Laskar et al., 2011) and to North Atlantic SST from core MD03-2699 (D, Rodrigues et al., 2012). Blue arrows indicate major cold events in the MD03-2699 record as defined by Rodrigues et al. (2012). Black dashed lines indicate points chosen for tuning the Sulmona $\delta^{18}O$ depth series to the MD03-2699 chronology.

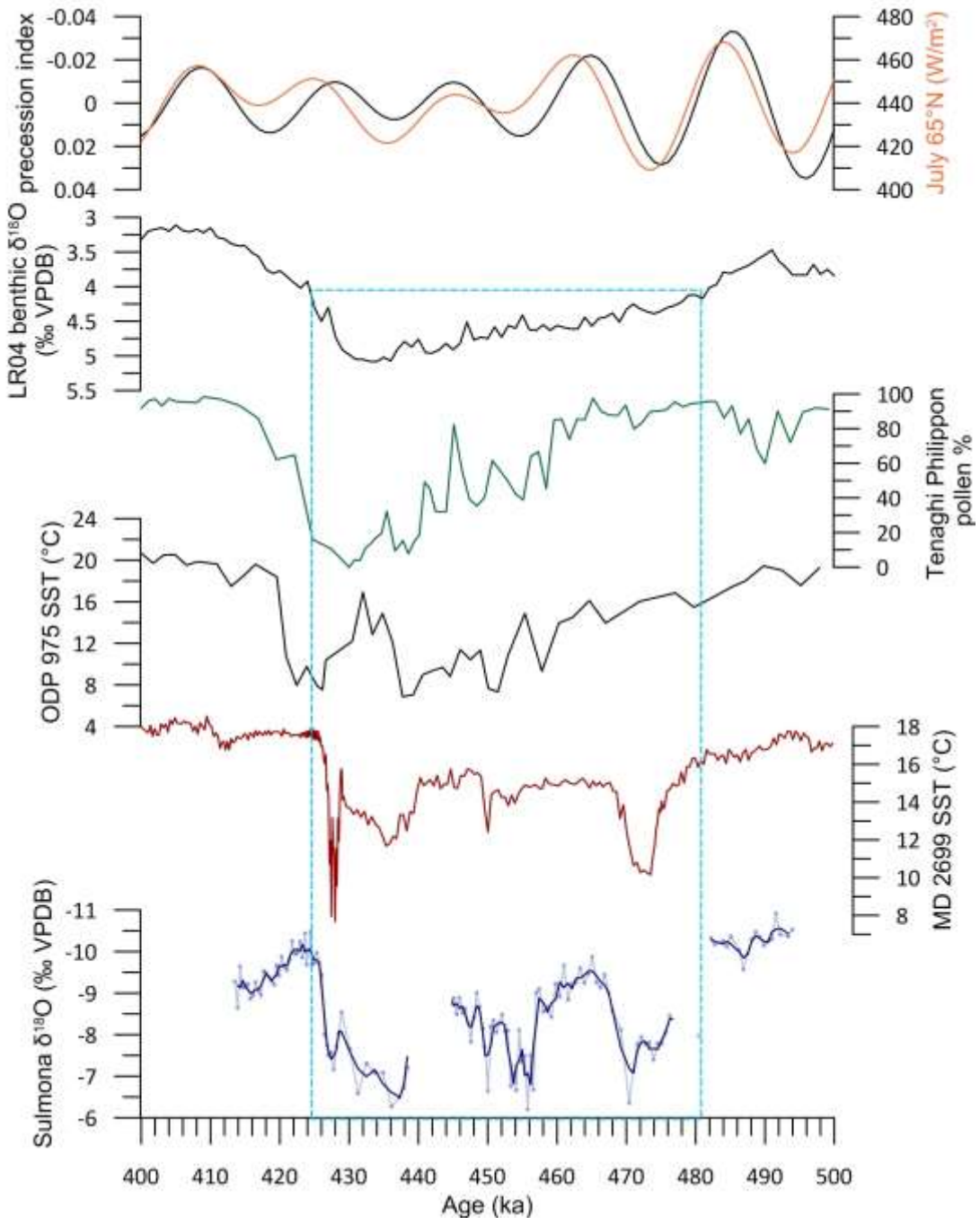

Figure 8- A) Sulmona record plotted on the proposed age model based on tephra layers and tuning points from MD03-2699 (see text and Fig. 7). B) Alkenone SST from core MD03-2699, Iberian margin (Rodrigues et al., 2012); C) SST from foraminifera assemblages, core ODP 975, western Mediterranean (Girone et al., 2013); D) Arboreal pollen % from Tenaghi Philippon, Greece (Tzedakis et al., 2006); E) LR04 benthic stack (Lisiecki and Raymo, 2005); F) July insolation at 65°N (red) and

precession index (black), Laskar et al., 2011. Light blue dashed rectangle indicates the interval with benthic $\delta^{18}O$ values lower than 4.15 ‰.